Department of AERONAUTICS and ASTRONAUTICS
STANFORD UNIVERSITY

Third Semiannual Progress Report

ADDITIONAL STUDY AND FURTHER DEVELOPMENT OF THE TRACER-SPARK TECHNIQUE FOR FLOW-VELOCITY MEASUREMENTS

Contract No. NsG-620

Subject:

A Study of Temperature, Ionization Level,
and Electron Energy in Sparks Used
for Flow-Velocity Measurements

by
James B. Kyser

Submitted to the

National Aeronautics and Space Administration
by the
Department of Aeronautics and Astronautics

Stanford University
Stanford, California

December 1965

Third Semiannual Progress Report

ADDITIONAL STUDY AND FURTHER DEVELOPMENT OF THE TRACER-SPARK TECHNIQUE FOR FLOW-VELOCITY MEASUREMENTS

Contract No. NsG-620

Subject:

A Study of Temperature, Ionization Level,
and Electron Energy in Sparks Used
for Flow-Velocity Measurements

by
James B. Kyser

Submitted to the

National Aeronautics and Space Administration
by the
Department of Aeronautics and Astronautics

Stanford University

Stanford, California

December 1965

I. SUMMARY

As part of a general study of the behavior of a spark-heated column of gas in a hypersonic stream, time-resolved measurements of spark temperature and intensity profile have been made in a static test chamber for a range of spark energies and static pressures. In addition, the effects of a magnetic field parallel to the spark axis have been investigated. On the basis of these static measurements, electric field strength, electron energy, and ionization level have been computed. The results show that a low voltage gradient and a low electron temperature exist in the spark at its mid-duration. Ionization level is high, particularly in the case of high magnetic field strength and low static pressure. On the assumption that the initial conditions for the spark-heated column are given by the average conditions during the spark lifetime, the starting point in the study of the spark-heated column behavior has been established.

An analysis of the spark process indicates that the rate of increase of translational-rotational temperature has a maximum value at an electric field strength of 1.0 to 1.5 volts/cm/mm Hg and is rather insensitive to changes in field strength. Furthermore, the maximum computed value is only about 60% of the measured rate of increase of temperature. Preliminary analysis shows that rotational non-equilibrium effects could be responsible for this discrepancy. Further work will be required in order that a better measurement of electric field strength can be obtained.

II. INTRODUCTION

The measurement of stream properties in a hypersonic wind tunnel is a difficult problem that has occupied many investigators for a number of years. Although the techniques of obtaining stagnation-point properties, such as pressure and heat-transfer rate, are well understood, there is a great deal of uncertainty concerning measurements of stream properties in the undisturbed stream. Karamcheti et.al. (1962) have shown the importance of an accurate knowledge of stream velocity by considering the effects on measurements of other quantities caused by an erroneous

computation of velocity. They have also shown that the stream velocity can not necessarily be obtained from measurements made in the tunnel reservoir and in the stagnation region.

Numerous methods of measuring flow velocity in hypersonic tunnels have been used. These include the measurement of the convection of a spark-generated blast wave used by Karamcheti et.al. (1962). More recently, the convection of the actual spark-heated column has been measured to obtain flow velocity. Kyser (1964) measured the convection of the spark-heated column by striking a second spark through the column, relying on the residual ionization of the column to provide a perferential path. Cunningham and Dicks (1964) used microwaves to measure the convection of the spark-heated column, with the residual ionization of the column attenuating a microwave signal transmitted across the stream. Fuller (1965) measured the convection of the spark-heated column with photomultipliers, the residual emission of radiation several microseconds after the spark was extinguished giving the detectable signal.

These three techniques depend on the spark-heated column being convected in exactly the same manner as the undisturbed stream and hence are subject to some question. Ruginger (1964) pointed out that the spark-heated column follows the gas velocity only if the velocity is constant and that in the extreme case the column velocity can exceed the gas velocity by as much as 60% if the gas is accelerated by a moving shock wave. Cunningham and Dicks (1964) noted that their technique gave invalid velocity measurements when an excessive amount of energy was used to generate the spark. Also, it is apparent that both thermal expansion and ion diffusion can severely reduce the measuring accuracy obtainable with any technique that relies on the measurement of the location of the spark-heated column at some later time.

The present study of the behavior of a spark-heated column of gas in a hypersonic stream was undertaken to help clear up these uncertainties and thus provide a basis for estimating the accuracy of velocity measurements that depend on the convection of the spark-heated column. The study is composed of two parts. First, the spark process will be studied to establish the conditions in the spark-heated column at the instant

the spark is extinguished. Second, the subsequent motion of the spark-heated column will be studied, using the conditions obtained from the spark studies as initial conditions. This report deals with the first part of this study, the measurement of the initial conditions in the spark-heated column. The subsequent motion, i.e., thermal expansion and diffusion, will be covered in the final report. Since the duration of the spark is short compared with the period of time used for measuring the convective velocity of the spark-heated column, the initial conditions in the spark-heated column will be assumed to be given by the average conditions existing during the spark, and spark processes will be considered only because of their ultimate effect on the initial spark-heated column conditions.

The program of measuring the initial conditions of the spark-heated column was conducted in a static-test chamber rather than in the hypersonic stream in the wind tunnel because of the large number of measurements required and the difficulty of controlling and repeating stream conditions in successive tests. The static-test chamber is shown in Figure 1. The chamber was attached to the tunnel vacuum tank so that the tunnel vacuum system and pressure gages could be used in the static tests. The large pumping capacity of the tunnel vacuum system made it possible to flush the test chamber continuously with bottled nitrogen to keep the test gas pure.

The circuit used to generate sparks for the static tests is the same circuit used in previous work (Kyser, 1964) and is shown in Figure 2. Spark energy was varied by changing the size of the storage capacitor. When the smallest capacitor was used, it was found that the capacitance of the transmission cable altered the discharge characteristics because of its contribution to the LC product of the circuit. To alleviate this, the transmission cable was made as short as possible by placing the spark-generating circuit adjacent to the static-test chamber.

In earlier studies of the utility of using sparks for flow-velocity measurements, it was found that a magnetic field oriented parallel to the spark axis could cause a significant reduction in the diameter of the spark. Therefore, two coils were attached to the static-chamber

wall so that the effects of a magnetic field on the initial conditions of the spark column could be studied. The coils were accurately aligned, with their common axis containing the electrode axis. Power was obtained from a bank of twelve 12-volt aircraft batteries connected in series.

Static tests were conducted over a wide range of conditions so that results would be as general as possible. Spark strength was varied from 0.05 to 5.0 joules, magnetic-field strength from 0 to 655 gauss, and pressure from 0.1 to 10 mm Hg. Spark voltage and electrode gap were held constant respectively at 10 KV and 5 inches for all tests.

The measurements made in the static test chamber can be divided into three categories: spark current, spark temperature, and spark-intensity profile. Extensive quantitative current measurements were not made; it was thought sufficient to show that the current followed the light output closely. Extensive measurements of spark temperature and intensity profile were made, particularly in the case of the 0.5-joule spark at 1 mm pressure. Details of the techniques used are discussed in the following sections. On the basis of these measurements and certain assumptions, it was possible to compute the initial values of the parameters that govern the behavior of the spark-heated column. These computations and their implications are discussed in this report, but the details of the subsequent spark-column motion will not be covered until the final report.

III. MEASUREMENT OF SPARK TEMPERATURE

As a starting point in the study of the behavior of a spark-heated column of gas, the initial gas temperature must be measured. In principle, time-resolved measurements of spark temperature can be used to obtain the initial gas temperature by equating the final spark temperature to the initial temperature of the gas in the spark-heated column. Because of the sub-microsecond spark durations encountered in the work, it was necessary to resort to spectrographic measurements to obtain the required speed of response.

Nitrogen was selected as the test gas in the studies because it is

used for testing in the Stanford spark-heated hypersonic tunnel in order to avoid oxidation of the tunnel components and consequent contamination of the flow. Typical spectrographic plates of the nitrogen-spark spectrum are shown in Figure 3. From the plates it can be seen that the most prominent feature of the nitrogen-spark spectrum is a series of regularly spaced bands, called the second positive band system. The band system results from a single electronic transition, called the $C^3\pi_u \rightarrow B^3\pi_g$ transition in the terminology of spectroscopy. The B and C have no physical significance, but the superscript 3 indicates that the molecular states are triplet states, the π indicates that the quantum number of the electronic orbital angular momentum along the inter-nuclear axis is unity. The physical significance of the "u" and the "g" is not pertinent to this report. Each band results from a particular vibrational transition taking place simultaneously with the electronic transition, and close examination of each band would show that it is composed of a large number of lines rather than a continuum. Each line represents a particular rotational transition taking place simultaneously with the electronic and vibrational transitions. These lines can be grouped into branches called the "P" , "Q" , and "R" branches corresponding to a change in rotational quantum number of +1 , 0 , and -1 , respectively. Other values for the change in rotational quantum number are forbidden. Since the strength of each line is primarily a function of the number of molecules undergoing the corresponding transition, the rotational temperature can be found from the measured intensity distribution within a specified band. The correspondence between rotational temperature and the rotational quantum number for mean rotational kinetic energy can be seen from Figure 4. Room-temperature nitrogen in either the ground state or the excited state $C^3\pi_u$ has a mean rotational quantum number between 9 and 10. For both states, an increase of one in mean rotational quantum number corresponds to an increase of about $80^\circ K$ in rotational temperature. Translational temperature can be assumed equal to rotational temperature for most processes because of the small number of molecular collisions required for equilibration. The validity of this assumption will have to be examined further once the collision rates in the spark have been estimated.

Computed Intensity Distribution

Before temperature can be obtained from band-intensity distributions measured experimentally, it is necessary to compute intensity distributions from molecular constants for a range of rotational temperatures. The derivation of the equations governing emission of radiation by a molecular transition is well covered by Hertzberg (1950) or in references cited by him, so it will not be repeated here.

The frequency and wavelength of radiation from an electronic transition are related to the energy difference between the two states in the transition through Planck's relation

$$E = h\nu' = \frac{hc}{\lambda}$$

where E is the energy of the radiation, equal to the energy difference between the upper and lower states,

h is Planck's constant,
ν' is the frequency of the radiation,
C is the velocity of light, and
λ is the wave length of the radiation.

As a result of the size of the numbers involved, it is more convenient to work with wave number rather than frequency, where wave number is defined as

$$\nu = c\nu' = \frac{1}{\lambda}$$

Equations for the wave numbers of the lines in the three branches are given by Hertzberg as equations (IV-32) through (IV-34) and are as follows:

R branch: $\nu = \nu_o + 2B'_v + (3B'_v - B''_v)\, J + (B'_v - B''_v)\, J^2$

Q branch: $\nu = \nu_o + (B'_v - B''_v)\, J + (B'_v - B''_v)\, J^2$

P branch: $\nu = \nu_o - (B'_v - B''_v)\, J + (B'_v - B''_v)\, J^2$

where ν_o is the wave number of the band origin,

B_v is the reciprocal of the moment of inertia of the molecule in the vibrational state v (B'_v, upper state; B''_v, lower state), and

J is the rotational quantum number of the lower state of the transition.

The three equations can be written in terms of the upper-state rotational quantum number by the following substitutions:

R branch: $J = J' - 1$

Q branch: $J = J'$

P branch: $J = J' + 1$

This gives as a final result

$$\text{R branch:} \quad \nu = \nu_o + 2B'_v (J'+1) + (B'_v - B''_v)(J')(J' + 1) \qquad (1a)$$

$$\text{Q branch:} \quad \nu = \nu_o + (B'_v - B''_v) J' + (B'_v - B''_v) J'^2 \qquad (1b)$$

$$\text{P branch:} \quad \nu = \nu_o - (B'_v + B''_v)(J'+1) + (B'_v - B''_v)(J'+ 1)^2 \qquad (1c)$$

The terms B'_v and B''_v are evaluated with the aid of equation (III-114) of Hertzberg:

$$B_v = B_e - \alpha_e(v + 1/2) \qquad (2)$$

where B_e is the reciprocal of the moment of inertia of the molecule at equilibrium nuclear separation, and

$-\alpha_e(v + 1/2)$ is the correction for increase in nuclear separation resulting from anharmonic vibration.

Now it is necessary to select a particular band and thus fix the vibrational quantum numbers of the upper and lower states in the transition. Referring back to Figure 3 we see that the strongest bands have band heads at about 3370A, 3580A, and 3800A. In the work of Nicholls (1964) these are seen to correspond to the 0,0 ($v' = 0$, $v'' = 0$) band at 3371.3A, the 0,1 band at 3576.9A and the 0,2 band at 3804.9A. The 0,2 band was selected for the temperature measurements because of the better sensitivity of available photomultiplier tubes to the longer wavelength radiation. For the 0,2 band, equation (2) can be rewritten as

$$B'_v = B'_e - 1/2\ \alpha'_e$$

$$B''_v = B''_v - 5/2\ \alpha''_e$$

From Table 39 of Hertzberg, we obtain

$$B'_v = 1.8259 - 1/2(0.0197) = 1.8161 \quad [C^3\pi_u \text{ state}]$$

$$B''_v = 1.6380 - 5/2(0.0184) = 1.5920 \quad [B^3\pi_g \text{ state}]$$

With these values, equations (1) can be rewritten as

$$\text{R branch:} \quad \nu = \nu_o + 3.6518\ (J' + 1) + 0.2241\ (J')\ (J' + 1) \qquad (2a)$$

$$\text{Q branch:} \quad \nu = \nu_o + 0.2241\ (J')\ (J' + 1) \qquad (2b)$$

$$\text{P branch:} \quad \nu = \nu_o - 3.4081\ (J' + 1) + 0.2241\ (J' + 1)^2 \qquad (2c)$$

At this point it should be noted that ν_o is not the wave number corresponding to the band head at 3804.9A, which has a value of 26,282, but is the wave number of the band origin, i.e., the wave number of the $J' = 0$, $J'' = 0$ transition. The band head is formed by the P branch doubling back on itself. The difference in wave number between the band origin and the band head can therefore be found by differentiating equation (2c) and solving for the value of J' that makes the differential equal to zero. Thus we obtain

$$\frac{d\nu}{dJ'} = -3.4081 + .4482\ (J' + 1) = 0$$

or, $J' = 6$ or 7 since only integral numbers are not permitted. Therefore, we have

$$\nu_{\text{band head}} = \nu_o - (3.4081)\ (7) + (.2241)\ (7)^2$$

or $$\nu_o = 26{,}295\ .$$

If this substitution is made, equations (2) can be written as

$$\text{R branch:} \quad \nu = 26{,}295 + 3.6518\ (J' + 1) + 0.2241\ (J')\ (J' + 1) \qquad (3a)$$

$$\text{Q branch:} \quad \nu = 26{,}295 + 0.2241\ (J')\ (J' + 1) \qquad (3b)$$

$$\text{P branch:} \quad \nu = 26{,}295 - 3.4081\ (J' + 1) + 0.2241\ (J' + 1)^2 \qquad (3c)$$

Since wavelength may be measured more easily than wave number, equations (3) are more useful it put in terms of the wavelength λ by obtaining the reciprocal of each side. This is readily done with the help of the binomial theorem, as shown in the following for the R-branch equation:

$$\frac{1}{\nu} = \lambda = \frac{1}{26{,}295}\left[1 + \frac{3.6518}{26{,}295}(J' + 1) + \frac{0.2241}{26{,}295}(J')(J' + 1)\right]^{-1}$$

$$\lambda = \frac{1}{26{,}295}\left[1 - \frac{3.6518}{26{,}295}(J' + 1) - \frac{0.2241}{26{,}295}(J')(J' + 1) + \ldots\right]$$

$$\lambda = \left[3803.0 - 0.528\,(J' + 1) - 0.0324\,(J')(J' + 1)\right] 10^{-8} \text{ cm}$$

or

$$\lambda_N = 3803.0 - 0.528\,(J'_{RN} + 1) - 0.0324\,(J'_{RN})(J'_{RN} + 1) \text{ Angstrom units} \quad (4a)$$

Similarly for the Q branch we have

$$\lambda_N = 3803.0 - 0.0324\,(J'_{QN})(J'_{QN} + 1) \text{ Angstrom units} \quad (4b)$$

and for the P branch

$$\lambda_N = 3803.0 + 0.493\,(J'_{PN} + 1) - 0.0324\,(J'_{PN} + 1)^2 \text{ Angstrom units} \quad (4c)$$

where J'_{RN}, J'_{QN}, and J'_{PN} are the upper-state rotational quantum numbers corresonding to emitted radiation of wavelength λ_N.

At this point the line spacing within the band can be examined. It is readily seen that each branch has lines spaced as close as one-half an Angstrom unit at low rotational quantum numbers, and the P branch has a line spacing of one Angstrom unit at a rotational quantum number of 30.

In reality the line spacing is much closer than indicated by equations (4). This results from triplet splitting due to interaction of the electron spin vector with the electron orbital momentum vector. As a result, the lines are split into three lines, with an average wavelength given by equations (4). Owing to the close line spacing, the task of isolating, identifying, and measuring the intensity of a single line appears formidable. Therefore, for these studies the line structure

of the band was assumed to be a continuum. The intensity of the continuum at a particular wavelength was then assumed to be a function of the following factors:

a) the spacing of the lines in each branch at the given wavelength,
b) the line strengths in each band at the given wavelength,
c) the number of molecules with rotational quantum numbers corresponding to transitions that give rise to lines at the given wavelength.

This procedure implies that the energy of the radiation emitted by each molecule undergoing the specified electronic-vibrational-rotational transition is the same regardless of the rotational levels involved. It also implies that the probability that the upper-state molecule undergoes a transition is not a function of rotational quantum number. Strictly speaking, neither assumption is correct since both radiant energy and transition probability are functions of the wavelength of emitted radiation. Since the bands under consideration are narrow, however, a good approximation can be obtained with these two assumptions. The calculation of the three factors enumerated above will be covered in the following paragraphs.

The line spacing in each branch is found by the following procedure:

a) For a given wavelength λ_N, solve equations (4) for J_{RN}, J_{QN}, J_{PN}. As a result of the assumed continuum distribution, non-integral values of J can be allowed.

b) Solve for λ_R, λ_Q, and λ_P for $J_R = J_{RN} + 1$, $J_Q = J_{QN} + 1$, and $J_P = J_{PN} + 1$

c) Obtain the line spacing for the three branches from

$$\Delta\lambda_{RN} = \lambda_N - \lambda_R \tag{5a}$$

$$\Delta\lambda_{QN} = \lambda_N - \lambda_Q \tag{5b}$$

$$\Delta\lambda_{PN} = \lambda_N - \lambda_P \tag{5c}$$

This procedure will not be valid in the space between the band origin and the band head because there the P branch has two values of J_{PN}

corresponding to each λ_N . Since this space represents a range of less than 2 Angstrom units in width, the restriction is of little consequence.

Both upper and lower states in the transition have a value of Λ of unity. Therefore, the line strengths are given by equations (IV-81) of Hertzberg. These are

$$\text{R branch:} \quad S_{JR} = \frac{(J' + 1)(J' - 1)}{J'} \tag{6a}$$

$$\text{Q branch:} \quad S_{JQ} = \frac{(2J' + 1)}{J'(J' + 1)} \tag{6b}$$

$$\text{P branch:} \quad S_{JP} = \frac{(J' + 2)(J')}{J' + 1} \tag{6c}$$

If the three line strengths for a given J' are added, the sum will be the level's statistical weight $(2J' + 1)$. Therefore, if a molecule undergoes a transition, the probability that the transition will be an R-branch transition, a Q-branch transition, or a P-branch transition will be

$$\frac{S_{JR}}{2J' + 1}, \quad \frac{S_{JQ}}{2J' + 1}, \text{ or } \frac{S_{JP}}{2J' + 1}, \text{ respectively.}$$

The number of molecules at a given rotational quantum number is found with the aid of equation (III-167) in Hertzberg:

$$N_J = N \frac{hcB}{kT} (2J + 1) e^{-\frac{BJ(J + 1)hc}{kT}} \tag{7}$$

where N is the total number of molecules,
h is Planck's constant,
c is the velocity of light,
B is B_v used earlier to evaluate line position,
k is Boltzmann's constant, and
T is the temperature in degrees K .

For a given sample of gas at a specified temperature, equation (7) can be rewritten as

$$N_J = K_1(2J' + 1) e^{-\frac{B'_v J'(J' + 1) hc}{kT}}$$

$$= K_1 (2J' + 1) \exp\left[- \frac{(2.607)\ (J')\ (J' + 1)}{T} \right]$$

where the constant K_1 is the same for all rotational quantum numbers and the prime notation refers to the upper state as noted earlier.

Combining these factors, we can write the continuum intensity at any wavelength λ as

$$I_N = I_{RN} + I_{QN} + I_{PN} \tag{8}$$

where

$$I_{RN} = K_2 \frac{S_{RN}}{\Delta\lambda_{RN}} \exp\left[- \frac{(2.607)\ (J'_{RN})\ (J'_{RN} + 1)}{T} \right]$$

$$I_{QN} = K_2 \frac{S_{QN}}{\Delta\lambda_{QN}} \exp\left[- \frac{(2.607)\ (J'_{QN})\ (J'_{QN} + 1)}{T} \right]$$

$$I_{PN} = K_2 \frac{S_{PN}}{\Delta\lambda_{PN}} \exp\left[- \frac{(2.607)\ (J'_{PN})\ (J'_{PN} + 1)}{T} \right]$$

and

K_2 is a constant for a given sample of gas at specified temperature, and is a function of band intensity corresponding to a line spacing of unity,

S_{RN}, S_{QN}, and S_{PN} are given by equations (6a), (6b), and (6c),

$\Delta\lambda_{RN}$, $\Delta\lambda_{QN}$, and $\Delta\lambda_{PN}$ are given by equations (5a), (5b), and (5c),

J_{RN}, J_{QN}, and J_{PN} are the solutions to equations (4a), (4b), and (4c) for a specified wavelength λ_N, and

T is the specified temperature.

On the basis of equation (8), values of I_N were calculated for values of λ_N from 3802 to 3755 Angstrom units, the head of the next band. These values, normalized with respect to the intensity of 3795 Angstroms, are shown in Figure 5 for selected temperatures between 200°K and 2000°K. The reasons for selecting this normalization procedure will be discussed in the following section.

Experimental Method

The spark spectrum was analyzed with either a Hilger medium quartz

spectrograph with a focal length of 0.6 meters or a Jarrel Ash half-meter spectrometer. The two instruments complemented each other in the following manner: the spectrograph permitted intensity-versus-wavelength data to be obtained at a given time or over a given time interval; the spectrometer permitted intensity-versus-time data to be obtained at a given wavelength or over a given wavelength interval. Because of the low spark-light levels, it was necessary to have a time interval of at least the duration of the spark when the spectrograph was used to collect data. As discussed in the previous section, it was necessary to have a wavelength interval greater than the rotational line spacing when the spectrometer was used.

Spectrographic plates of a 0.5-joule spark at 1.0 mm pressure are shown in Figure 3. The upper three spectra correspond to 5, 25, and 125 sparks with no magnetic field. The lower three spectra correspond to 1, 5, and 25 sparks with a 655-gauss magnetic field. Data obtained in this manner permit the entire spectrum to be examined relatively easily. The experimental arrangement used to obtain spectrographic data is shown in Figure 6. The collimating lens was glass and hence probably filtered out all radiation with wavelengths shorter than 3000 Angstrom units.

The apparatus used to obtain data with the spectrometer is also shown in Figure 6. The spectrometer was removed as far as possible from the spark to reduce the effects on the data of RF radiation from the spark. Collimating and condensing lenses were used to achieve a maximum light-gathering efficiency. The geometry of the optical path also provided a maximum selectivity of light from the spark. The optical components were adjusted with the aid of a neon bulb inserted in place of the spark column, and the image of the center of the bulb was focused on the entrance slit.

A Dumont 6292 photomultiplier tube was used to measure the light-intensity at the exit slit of the spectrometer. A diagram of the circuit used with the tube is shown in Figure 7. To minimize noise pickup, all leads were kept as short as possible and the entire circuit was encased in a brass tube. A mu-metal shield was placed around the photomultiplier tube as a further precaution. The output resistance was kept as small as possible, 1000 Ohms, to insure a satisfactory response time.

Data were recorded on a Tektronix type-551 oscilloscope in conjunction with a type-53/54B preamplifier. The preamplifier had an input capacitance of 47 pf, and the coaxial data cable had a distributed capacitance of about 34 pf. Therefore, the RC product of the photomultiplier output circuit was 0.08 microseconds, which is 60% greater than the molecular upper-state lifetime.

The linear range of the photomultiplier circuit was found by inserting calibrated neutral-density filters in the optical path and observing the effect on the output. As a result of this procedure it was found necessary to limit photomultiplier output to 60 millivolts or less, which corresponds to an anode current of 60 microamps or less.

The spark was oriented along a horizontal line so that it was at right angles to the spectrometer slit. Preliminary experiments showed that if the spark were oriented parallel to the slit, large random variations in intensity would occur, indicating a spatial instability of the spark. These variations were greatly reduced by orienting the spark at right angles to the slit and opening the slit to its maximum height and width.

The large slit widths used made it necessary to modify the computed intensity distributions shown in Figure 5 to account for the instrument-profile effects, that is to account for the fact that the photomultiplier tube was measuring the intensity of radiation over a wide range of wavelengths rather than at a single wavelength. Instrument profile was measured by setting the spectrometer slit width and slit height to the values used in the experiments and scanning the 6328-Angstrom line from a helium-neon laser. The results, plotted as intensity ratio versus wavelength, are shown in Figure 8. Since the laser line has virtually zero line width, the data shown give the actual instrument profile without correction for line profile. The instrument profile shown in Figure 8 was assumed to apply at a wavelength 3805 Angstrom units without correction for the change in wavelength.

The band-intensity distribution data were corrected for instrument-profile effects by assuming that the relative instrument response was as

follows:

100% at $\lambda = \lambda_{set}$

74% at $\lambda = \lambda_{set} \pm 2$ Angstrom units

39% at $\lambda = \lambda_{set} \pm 4$ Angstrom units

0% at $\lambda = \lambda_{set} \pm 6$ Angstrom units

Intensity distributions corrected in this manner are shown in Figure 9 for temperatures between 200°K and 2000°K. These values are what would be measured if gas samples at the indicated equilibrium temperatures were examined with the spectrometer.

Preliminary surveys of the intensity distribution across the entire band have been made of the 0.5-joule spark at 1 mm pressure. These data, which are not included in this report, indicate that the gas in the spark is close to equilibrium, that is, that the distribution of rotational kinetic energy is close to an equilibrium distribution.

If the gas in the spark has an equilibrium distribution of rotational kinetic energy, the rotational temperature can be found by measuring the band intensity of any two wavelengths. It can be assumed then, that the translational temperature is in equilibrium with the rotational temperature, and therefore the temperature found in this manner is the temperature in the equation of state of the gas. For the case under discussion, 3795 Angstrom units appears to be a convenient value for one of the two wavelengths because the computed intensities can not be considered reliable at wavelengths much closer to the origin. With this in mind, the corrected band intensities at 3775 Angstrom units and 3785 Angstrom units have been divided by the corrected intensity at 3795 Angstrom units and plotted versus temperature in Figure 10. For the present study, the 3785-Angstrom curve is the more desirable because of its steeper slope in the 300°K to 400°K temperature range.

Spark temperatures were obtained by recording the time-resolved band intensities at 3795 and 3785 Angstrom units. Figure 10 was used to convert the ratio of intensities to temperature. The band intensities at the two different wavelengths could not be measured simultaneously,

so it was necessary to utilize a separate spark for each measurement. A continuum radiation, presumed due to transitions involving free electrons, was found to exist in the spark spectrum. The intensity of the continuum did not appear to vary with wavelength, so it was measured by setting the spectrometer at 3815 Angstrom units, which is 10 Angstrom units beyond the band head. As a result, each spark temperature measurement took three sparks, one with the spectrometer set at 3815 Angstrom units, one at 3795 Angstrom units, and one at 3785 Angstrom units. A second photomultiplier tube with a circuit similar to Figure 7 was used to insure that the spark liminousity was the same for each spark.

Experimental Results

On the basis of the procedure described in the previous paragraphs, spark temperatures were measured for the following conditions:

spark energy: 0.05, 0.5, 5.0 joules
magnetic field: 0, 225, 445, 655 gauss
pressure: 0.1, 0.33, 1.0, 3.0, 10 mm Hg.

All tests were conducted in the static test chamber, and the chamber was flushed with nitrogen between sparks to insure that the test gas did not become contaminated. Oscillograms obtained with each of the spark energies are shown in Figure 11. The upper set of traces in each case is the data; the lower trace is a composite of the monitor output from each spark. The data traces correspond, from top to bottom, to 3815, 3795, and 3785 Angstrom units. The horizontal and vertical scales are noted in the figure. The slight ripple in the data traces is due to radio-frequency radiation from the spark.

Time-resolved temperatures at the spark centerline obtained from similar oscillograms are shown in Figure 12 for a number of sets of 0.5-joule sparks at 1.0 mm pressure with magnetic field strengths of 0 and 655 gauss. In each case the static temperature appears to originate at a value somewhat higher than the ambient temperature of 295^{o}K. Some increase in temperature during the course of the spark can be noticed since the final temperatures are generally higher than the initial values. The rates of increase are not measurable in this form, however,

because of the scatter induced by the noise discussed earlier.

The lines in Figure 12 were obtained by curve-fitting an equation of the form

$$T = T_o + \frac{dT}{dt} t \qquad (9)$$

where T is the temperature in degrees Kelvin, and

t is the time in microseconds from the initiation of the spark

to each set of data by the least-squares technique. The resulting equations are

$$T = 354 + 18.4\ t \qquad (10)$$

for zero-gauss magnetic field strength, and

$$T = 340.5 + 93\ t \qquad (11)$$

for the 655-gauss case.

It is doubtful that the actual heating process had a constant increase of temperature with time. In view of the data scatter, however, a more elaborate temperature-time relationship was not justified. Nevertheless, the two fitted curves are consistent with each other in the time range between 0.15μs and 0.65μs in the following way:

1) At $t = 0.15\mu s$ the temperatures differ by 3 degrees, which is much less than the measuring accuracy.
2) The temperature-time slope for the spark with 655-gauss magnetic field is five times as great as the slope for the spark without magnetic field. This ratio is approximately the inverse of the ratio of spark cross-sectional areas, which implies that the rate at which energy is added to the gas by the spark is the same in each case.

From this discussion it appears that the temperature-time relationships established by curve fitting are sufficiently precise to permit further analysis of the spark process. The effect of using such a large number of data points has been a cancellation of the noise-induced data scatter.

An alternate method of eliminating noise effects is to integrate the data signal over a number of noise cycles. This approach, which

yields average values, was used to show effects of spark strength, pressure, or magnetic-field strength on spark temperature. Average temperatures were obtained by finding the area enclosed by the 3785-Angstrom and 3815-Angstrom traces and the area enclosed by the 3795-Angstrom and 3815-Angstrom traces. The ratio of these two areas was then converted to temperature by means of Figure 10. The average spark temperatures obtained by this method are shown in Figure 13 for the three spark energies studied. Each data point represents a separate measurement. The data are best interpreted physically as the temperature of the spark at its midpoint or point of maximum intensity. For each spark they show a clear trend of increasing average temperature with increasing density. The average temperature is seen to increase with increasing magnetic field strength for the 0.5- and 5.0 joule sparks but not for the 0.05-joule spark.

IV. MEASUREMENT OF SPARK-INTENSITY PROFILE

As a further step in the computation of the spark-column properties it was necessary to obtain the current density in the spark. This was done by starting with the observed correspondence between current and spark intensity and assuming that a similar correspondence exists between spark-intensity distribution and current-density distribution. The justification for this assumption will be discussed in the next section. Spark-intensity distribution was measured in two ways: directly with an optical system and a photo-multiplier tube, and indirectly by recording the image on film and reading the film density with a microphotometer or densitometer.

The direct measurement has the disadvantage that a separate spark is required for each measurement as the radius is varied. Time-resolved intensity distributions can be obtained, however. The photographic method permits a complete intensity profile to be obtained from a single spark, but does not give time-resolved measurements. It has the further disadvantage that data must be corrected for nonlinearity of the film response and for three-dimensional effects.

All spark-intensity profile measurements were made in the static

chamber shown in Figure 1. Spark energy and magnetic field strength were varied as in the spark temperature tests, but fewer pressure levels were used. Except for the data-recording instrumentation, the test procedure was the same as discussed in the previous chapter. The apparatus used for the direct measurement of spark-intensity profile is identical to that shown in Figure 6 except that the spectrometer was removed and the spark image was focused directly on the photomultiplier assembly. An optical filter was inserted in the optical path to eliminate all radiation except the second positive band system. An orifice plate with a 0.028-inch diameter orifice was placed at the focal point to increase the resolution of the system. Since the image was enlarged three times by the two lenses, the effective field of view was about 0.010 inches in diameter. The low f-number of the colliminating lens and the long optical path to the condensing lens assured a shallow depth of field, so no correction for three-dimensional effects was applied to the data.

Time-resolved intensity profiles of the 0.5-joule spark at 1.0 mm pressure without a magnetic field and with a 655-gauss magnetic field are shown in Figure 14. The large amount of scatter is probably due to a variation in centerline location between successive sparks rather than to an intensity variation, since total spark luminousity was monitored and found to be relatively constant. The data in Figure 14 show that the spark with a zero-gauss magnetic field is quite diffuse during its early stage and tends to become more confined as time progresses. The confining influence is probably the self-induced magnetic field. The spark with a 655-gauss magnetic field does not exhibit this behavior, indicating that the externally applied magnetic field is the more important confining influence.

Intensities integrated over the total spark duration are shown in Figure 15. These values should be equivalent to those obtained from photographic data corrected for film nonlinearity and three-dimensional effects. The data shown in Figure 15 will be used in conjunction with the spectrographically measured heating rates shown in Figure 12 for further computation of spark-column properties. The two sets of data are compatible since each represents an integral or average over most

of the spark duration.

Spark photographs were made with either a Fairchile type-F-296 oscilloscope camera attached to the chamber or a 4 x 5-inch Graflex camera mounted on a tripod. Polaroid type-46-L film was used in the oscilloscope camera; Eastman Commercial film and Tri-X film were used in the Graflex camera. The type-46-L film was found to be the most satisfactory, in spite of a nonuniformity in background opacity, because of its lower exposure threshold and consequent better linearity. The results of the photographic measurements of spark-intensity profile are shown in Figure 16 as normalized radii. All radii were normalized with respect to the radius of the 0.5-joule spark at 1 mm pressures without magnetic field. The data were not corrected for film nonlinearity and for three-dimensional effects because each of these corrections is subject to uncertainties. It is doubtful, therefore, that the accuracy of corrected data would be as good as that of the direct measurements.

The data-reduction procedure used to obtain Figure 16 was as follows: Films of all sparks were read with the microphotometer, and the areas under the intensity-distance records were obtained. Mean radius, defined as one-half this area divided by the peak intensity, for each spark was then normalized by dividing by the mean radius for the 0.5-joule spark at 1 mm pressure without magnetic field. This data-reduction procedure is based on the assumptions that the intensity-distance plots for all sparks have similar shape, and that film nonlinearity and three-dimensional effects are the same for all spark photographs.

The first assumption was varified by a comparison of the microphotometer records of the intensities of the photographed spark images. Four of these profiles are reproduced in Figure 17, normalized so that each has a peak intensity of unity. An inspection shows the intensity distribution to be a modified Gaussian curve, similar in shape for all profiles. As the magnetic field is decreased the curves are stretched along the distance axis but otherwise remain unchanged except for some distortion in the region of very low intensity ratios.

Film-nonlinearity effects were made constant from film to film by

holding the maximum exposure level constant. Thus, if the photographed intensity profiles were corrected, a specified intensity ratio in each profile would be multiplied by the same correction factor. Although the profiles would be distorted by such a correction, the curves would remain similar in shape if they were originally similar. Likewise, if similar curves were corrected for three-dimensional effects, the resulting curves would be similar in shape.

In view of the above discussion, it appears that a good approximation to the corrected spark-intensity profile for each of the conditions represented in Figure 17 can be obtained, if the ordinate in the zero-gauss intensity distribution in Figure 15 is multiplied by the corresponding normalized radius.

V. PROPERTIES OF SPARK-HEATED COLUMN DEDUCED FROM MEASUREMENTS

As discussed earlier, the primary purpose of the present study is the measurement and computation of the gas properties in the spark-heated column at the time the spark current ceases. These gas properties will be used in later phases of the research program as initial conditions in the study of the behavior of the spark-heated column in a hypersonic stream. The quantities that must be obtained through direct measurement or computed from measurements are gas temperature, electron energy, and electron concentration. Furthermore, these might not be constant across the spark column, so the radial variation as well as the value in the center of the spark must be obtained.

The two previous sections discussed the measurement of temperature at the center of the spark and the measurement of spark-intensity profile. From the latter, current density was inferred. The variation of temperature with radial distance is not known, and additional spectroscopic measurements of further analysis will be required before it can be established.

Electron energy and concentration are functions of electric field strength and can be obtained if electric field strength is known. Although the electric field strength cannot be measured directly, it can be obtained from the rate at which energy is added to the gas by the

spark if the current density is known.

Rate of Energy Addition

The rate of energy addition is found from the heating-rate data in Figure 12, where the rates of change of temperature with time were 18.4×10^6 °K/sec for the 0.5-joule spark at 1 mm pressure without field and 93×10^6 °K/sec for the same spark with a 655-gauss field. These values are average values over the portion of the spark between 0.15μs and 0.65μs as a consequence of the assumed temperature-time relationship used in curve-fitting the spectroscopic data.

As discussed in Chapter III, the temperature actually measured was the rotational temperature. Since the translational temperature and the rotational temperature equilibrate in a few molecular collisions, for the present this heating-rate data can be assumed to be indicative of the change in the translation temperature with time. Owing to the long relaxation times associated with vibrational and electronic temperatures, there is probably no relationship at this gas density and spark duration between the amount of vibrational and electronic energy added to the gas and the measured heating rate. It follows then that the measured heating rate can be used to compute the energy added to the gas by translational and rotational excitation only.

When an element of gas undergoes a constant-volume heating process, the rate of energy addition and the rate of temperature increase are related by

$$\frac{dQ}{dt} = \rho c_v \frac{dT}{dt} \tag{12}$$

where $\frac{dQ}{dt}$ is the rate of energy addition,
ρ is the gas density,
c_v is the specific heat per unit mass at constant volume, and
$\frac{dT}{dt}$ is the rate of temperature increase.

If we want to relate the change in energy represented by rotational and translational excitation to the change in rotational-translational

temperature, we can use the values c_v for room-temperature gas, since only these two modes are excited at low temperatures. The specific heat at constant volume is used because it appears that the gas in the spark will not be able to expand appreciably during the 0.8-microsecond spark duration, even though some heating might occur.

For nitrogen at a temperature of 295°K and a pressure of 1 mm, we have

$$\rho = 1.55 \times 10^{-6} \text{ gm/cm}^3$$

$$c_v = 0.177 \text{ cal/gm}^\circ\text{K} = 0.74 \text{ joules/gm}^\circ\text{K} .$$

On the basis of these values and the heating-rate data from Figure 12, the energy added to the translational and rotational degrees of freedom is calculated as

$$\frac{dQ}{dt} = 21.1 \text{ joules/cm}^3\text{sec} \qquad \text{without magnetic field}$$

$$\frac{dQ}{dt} = 107 \text{ joules/cm}^3\text{sec} \qquad \text{with 655-gauss field}$$

It should be noted again that these values do not include the energy added to the gas through vibrational and electronic excitation.

Current Density

Current density is found from the spark-intensity profiles in Figures 14 and 15 by assuming a proportionality between intensity and current density. This assumption can be justified on physical grounds. As discussed earlier, measurements of spark current and spark luminosity showed that the luminosity was proportional to current. Massey and Burhop (1952) give the excitation cross section for the nitrogen second positive band system and show it to be zero for electron energies less than 14 electron volts and to reach a maximum at 20 electron volts. Consequently, only a small percentage of the total number of electrons is capable of exciting this band system. The radiation produced is proportional to the number of excitation collisions, which is a function of the number of electrons and their temperature. If the electron temperature is uniform across the spark as indicated by von Engle (1955), the luminous intensity will be proportional to the electron concentration.

A uniform electron temperature implies a uniform field strength and consequently a uniform electron drift velocity. Therefore, current density will be proportional to electron concentration and hence proportional to luminous intensity. Since the number of electrons with sufficient energy for excitation is small, the number of molecules excited will be small compared with the total number of molecules. Even though each molecule can undergo only one excitation-emission cycle during the spark, the number of molecules available for excitation will not be affected by the number of previous excitation collisions.

For these computations of current density, the integrated intensity profile found in Figure 15 must be used to be consistent with the average heating-rate data. The constant of proportionality between intensity and durrent density oan be found by equating the total current to the product of the constant of proportionality and the volume under the intensity-radius curve. That is, we can write

$$I_t = K \int_0^R 2\pi r \, I(r) \, dr \qquad (13)$$

where I_t is the total current,
K is the constant of proportionality,
R is the maximum radius of the spark column,
r is the radius, and
$I(r)$ is the local value of intensity from Figure 15.

This procedure assumes, of course, that the spark-intensity profile is axisymmetric about the point $r = 0$.

A value of $I_t = 0.80\ I_{max} = 168$ amps was chosen to be consistent with the average heating rate used. This value corresponds to the average current during the time interval between 0.15 and 0.65μs . When the integration in Eq. (13) was performed graphically, the following values of K were obtained:

$K = 16$ amp/cm^2/unit of intensity — without magnetic field,
$K = 80$ amp/cm^2/unit of intensity — with 655-gauss field.

The maximum values of current density corresponding to these values are

$I = 16$ amp/cm^2 without magnetic field,

$I = 80$ amp/cm^2 with 655-gauss field.

The heating rates found earlier can be divided by the appropriate value of current density to give heating rate for a unit current density. For both cases the result is

$$\frac{dQ}{dt} = 1.32 \text{ joule/cm}^3\text{sec} ,$$

which is equivalent to a voltage gradient of 1.32 volts per cm. The heating rate for unit current density can be put in more convenient units by use of the physical constant 1 joule = 6.23×10^{18} electron volts. This gives a heating rate of

$$\frac{dQ}{dt} = 8.2 \times 10^{18} \text{ electron volts/cm}^3\text{sec}$$

for unit current density.

Computation of Electric Field Strength

The relationships between electron behavior and electric field strength have been measured by a large number of investigators over the past 50 years. The results of investigations by Crompton and Sutton (1952) and by Townsend and Bailey (1921) are shown in Table I. These will be used in subsequent calculations.

As a first step, the electron concentration required by the current density can be found for each value of electric field strength listed in Table I. These two parameters and the electron-drift velocity are related by

$$I = n_e w q_e \qquad (14)$$

where I is the current density,

n_e is the electron concentration,

w is the electron-drift velocity, and

q_e is the electron charge, 1.602×10^{-19} coulomb .

Equation (14) has been solved for a unit current density (1 amp/cm^2) for each value of field strength listed in Table I; the resulting electron

concentrations are plotted in Figure 18. Electron collision information from Table I can now be used along with electron concentration to find gas heating rate as a function of electric field strength. In principle, the value of electric field strength corresponding to the measured heating rate will be the electric field strength in the spark.

The mechanics of electron-molecule collisions must be examined briefly to assure that the results are consistent with the restriction that the measured heating rate did not reflect the vibrational and electronic excitation energy that was being added to the gas.

According to simple kinetic theory, the maximum amount of energy that can be transferred to a nitrogen molecule through a single elastic collision with an electron is

$$\Delta E = \frac{2m}{M} \epsilon = .39 \times 10^{-4} \epsilon \qquad (15)$$

where ΔE is the energy added to the molecule,
m is the mass of the electron,
M is the mass of the molecule, and
ϵ is the kinetic energy of the molecule.

This result follows from the assumption of conservation of energy and momentum during the collision, and therefore the energy transferred will be translational kinetic energy only. Measurements of energy transfer obtained from electron-swarm experiments, as presented by Compton and Sutton (1952), show that the actual energy transfer is an order of magnitude higher than this value even at electron excitation energy levels well below the vibrational threshold.

Gerjuoy and Stein (1955) attribute this discrepancy to rotational excitation and show theoretically that, as a result of rotational excitation, the actual energy loss will be an order of magnitude greater than given by equation (15). From this discussion, it appears that the fractional energy loss per collision in Table I for low values of electron energy represents the fraction of energy that can be transferred by means of translational and rotational excitation. At higher values of field strength, the fractional energy transfer is higher because of vibrational and

electronic excitation. Shultz (1949) and Haas (1957) have shown the rapid increase in fractional energy transfer at electron energies near one volt to be due to an electron-attachment collision in which the negative ion N_2^- is formed. The ion has a short lifetime, and when the extra electron is rejected, a large part of the binding energy is transferred to vibrational excitation. Haas reports the collision cross-section for this phenomena to be sharply peaked at 2.3 electron volts, with a magnitude of about 15% of the elastic scattering cross-section. The cross-section is virtually zero outside the energy range between 1.5 and 5 electron volts. Electronic excitation does not become significant until electron energies are increased to above 15 electron volts, and so should not have much effect at the mean energies listed in the table.

From the above discussion we can construct the following model for electron collision processes in the spark:

a) Define an "active" collision as one that excites only molecular translation and rotation, the so-called active degrees of freedom. Define an inelastic collision as one that excites other modes, the inactive degrees of freedom.

b) Assume that the fractional energy transfer per collision due to active collisions does not change with increasing electron energy. Regardless of the electron energy, the equations of conservation of energy, linear momentum, and angular momentum must apply, and accordingly will limit fractional energy transfer.

c) Assume that the fractional energy transfer per collision for a mean electron energy of 0.1 ev , $\bar{\lambda} = 3.1 \times 10^{-4}$, is due entirely to active collisions, and that this is the appropriate value for active collisions regardless of electron energy level.

d) Assume that the number of inelastic collisions is small compared with the number of active collisions. Since the vibrational-excitation cross-section has a maximum value of 15% of the elastic-scattering cross-section, we can expect the number of inelastic collisions to be less than 15% of the number of active collisions,

or less than 13% of the total number of collisions. If we assume that an average of half of the electron energy is transferred during a single inelastic collision and that 10% of the collisions are inelastic, then we have a fractional energy transfer per collision of 500×10^{-4}. This value corresponds to an electron energy of 2.3 ev., and compares favorably with the tabulated value of 166×10^{-4} for a mean electron energy of 2.22 volts.

e) Assume that the molecular temperature increase measured spectroscopically is due only to energy transfer from active collisions. Energy transferred to molecules as vibrational or electronic excitation will not affect the translational or rotational excitation during the duration of the spark because of the long relaxation times associated with the internal degrees of freedom.

The energy added to the gas by electron collisions is

$$\frac{dQ}{dt} = n_e n_c \bar{\lambda} \epsilon \tag{16}$$

where n_c is the number of collisions per second per electron
$\bar{\lambda}$ is the fractional energy transfer per collision, and
ϵ is the mean electron energy in volts.

This may be rewritten as

$$\frac{dQ}{dt} = n_e \frac{5.9 \times 10 \sqrt{\epsilon}}{L} \bar{\lambda} \epsilon = \frac{5.9 \times 10 \, \bar{\lambda} n_e (\epsilon)^{3/2}}{L} \tag{17}$$

where L is the electron mean free path.

If a value of $\bar{\lambda} = 3.1 \times 10^{-4}$ is used for the fractional energy transfer due to all active collisions and appropriate values for ϵ and L are taken from Table I, the rate of increase of rotational and translational energy can now be found for each of the combinations of electric field strength and electron concentration given by Figure 18. These rates of increase are plotted in Figure 19 for the range of electric field strength given in Table I. The maximum value of electric field strength listed in the table corresponds to the sparking potential, so higher field strengths need not be considered since they cannot exist

for longer than about 10^{-9} seconds.

Two significant results are noted in Figure 19. First, the computed heating rate reaches a maximum at a field strength of about 1.2 volts/cm/mm Hg and decreases with further increase in field strength, implying that there is a maximum rate at which the translational-rotational temperature can be increased by a spark in nitrogen. Second, the measured heating rate of 8.2×10^{18} electron volts/cm^3sec is about 75% greater than the maximum computed heating rate.

In view of the above, it does not appear that without further study reliable electron-concentration and electron-temperature data can be obtained from spectrographic measurements of spark temperature. A "best guess" based on Figure 19 would be a value of 1.2 volts/cm/mm Hg for field strength, since this is the point of closest approach of the computed value to the measured heating rates. This value of field strength would give an electron energy of 1.0 ev. and an electron concentration of 1.2×10^{14} electrons per cubic centimeter for the zero-gauss spark. Since the gas density is 1.55×10^{-6} gm/cm^3, and each molecule has a mass of 46.6×10^{-24} gm, the molecular number density is 3.3×10^{16} molecules/cm^3, and the ionization level is 0.36%. For the 655-gauss spark, the electron concentration and ionization level are five times as large, or 6×10^{14} electrons per cubic centimeter and 1.8% respectively. From this it appears that the effect of the magnetic field is to concentrate the electrons in a more confined region, leaving the electric field strength and electron temperature unaffected.

A check of the magnitudes of the energy added to the various molecular degrees of freedom by electron collisions shows that the dissociation energy represented by the computed ionization is approximately equal to the energy added during the assumed constant-current portion of the spark. Since the dissociation energy was added during the 0.15-μs interval preceding the constant-current portion of the spark, it appears that half of the total energy added to the gas was added during the formative stage. Because of the small current during this period, a high electric field strength would be required for the energy addition to take place.

About half of the energy added during the assumed constant-current

portion was added to the active degrees of freedom. The remainder was added to the inactive degrees of freedom, primarily vibration. It can be seen that about three-quarters of the total energy added to the gas by the spark process was added to the inactive degrees of freedom and was not considered in the computation of spark heating because of the long relaxation time. This internal energy will have to be considered, however, in the 50-to 100-μs period during which the motion of the ionized column of gas is being studied.

VI. CONCLUSIONS

As a result of the insensitivity of the computed heating rate to electric field strength, it appears than an alternate method will have to be used to obtain electron energy and concentration. At present, probes seem to be the most favorable method. Since it is unlikely that data can be taken during the spark lifetime, the probes will be used to study the decaying plasma after the spark. Presumably average electron concentration in the decaying plasma will be obtained. Because of the relatively slow recombination rate, it is expected that these results can be used to find electron concentration in the spark. Electric field strength and electron energy can then be obtained from Figure 18 and Table I. Although the decay process might cause some error in the inferred spark conditions, the electron characteristics in the decaying plasma are of greater concern to the present research program than the electron characteristics in the spark.

The computed heating rate shown in Figure 19 introduces some doubt about the interpretation of the spark-temperature measurements. If there is a maximum rate at which a spark can increase the rotational-translational temperature of nitrogen for a specified current density, then the time-temperature relationship shown in Figure 14 cannot occur. The sudden initial increase of about $60^{\circ}K$ is not compatible with such a restriction. Furthermore, if the maximum heating rate predicted by Figure 19 is used to compute the final increase in temperature, a value of less than $10^{\circ}K$ is obtained for the 0.5-joule spark at 1 mm pressure without a magnetic field.

Although there might be some objection to the model used to obtain the computed heating rate, the behavior shown by the calculated values in Figure 19 can be explained on physical grounds. At electric field strengths above 1.2 volts/cm/mm Hg , the energy transfer to active degrees of freedom decreases because of the rapid increase in vibrational-excitation cross-section and the consequent increase in electron energy transferred to the vibrational degree of freedom. The presence of a large excitation cross-section has little effect on electron drift velocity, and therefore little effect on the electron density required to conduct the specified current density. Consequently, as the electric field strength increases, the number of electrons decreases monotonically as shown in Figure 18, and the electron energy increases much less rapidly as a result of the energy spent in vibrational excitation. The product $n_e(\epsilon)^{3/2}$ in Equation (16) decreases, causing dQ/dt to decrease.

A possible explanation for the measured heating rate being larger than the computed rate is seen by examining the assumption of equilibrium between the translational temperatures and the rotational temperature. It can be surmised on the basis of the discussion in the previous section that almost all of the active energy transferred to a molecule as a result of an electron collision is transferred to rotational excitation. About five molecular collisions are required before this increased energy is partioned equally between the five active degrees of freedom, so the relative frequence of electron-molecule and molecule-molecule collisions will give an indication of the state of equilibrium between the translational and rotational temperature.

If the values $L = 6.7 \times 10^{-3}$cm and $v = 4.2 \times 10^{4}$ cm/sec are used for molecular mean free path and mean thermal velocity, a molecule-molecule collision frequency of 6.3 collisions per molecule per micro-second is obtained. Similarly, if the values $L = 2.74 \times 10^{-2}$cm and $v = 5.92 \times 10^{7}$ cm/sec are used for electron mean free path and thermal velocity, an electron-molecule collision frequency of 2.16×10^{9} collisions per electron per second is obtained. Since the ionization level for the 0.5-joule spark without a magnetic field is 0.36%, each molecule will undergo 0.36×10^{-2} as many electron collisions, or 7.7 collisions per

microsecond. On the average, therefore, each molecule undergoes 1.2 electron-molecule collisions for each molecule-molecule collision, and as a consequence the rotational temperature will be higher than the translational temperature.

As discussed in the previous section, the mean electron energy is 1.0 electron-volt, and the average fractional energy transfer per collision to active degrees of freedom is 0.00031. The average active energy increase per electron collision would therefore be 0.00031 volts. If this energy went into the two rotational degrees of freedom only, it would cause a rotational temperature increase of $3.5^{\circ}K$ per collision, or $28^{\circ}K$ per microsecond. If this energy were equally distributed between the five active degrees of freedom, it would cause a rotational temperature increase of $1.4^{\circ}K$ per collision or $11^{\circ}K$ per microsecond. The measured increase of rotational temperature should fall somewhere between these two extremes. In fact it falls exactly half-way between.

The same reasoning can be used to give a possible explanation for the sudden temperature increase at the start of the spark. As discussed earlier, electrons exciting the second positive band system must have energies of about 20 electron-volts. If the mean fractional energy transfer to active degrees of freedom were 0.00031 for this electron energy level, then the mean energy transfer to active degrees of freedom during exciting collisions would be 0.0063 electron-volts. If this energy went into the two rotational degrees of freedom only, it would cause a temperature increase of $74^{\circ}K$. On the average, little of this energy would be transferred to the translational degrees of freedom before emission because the upper-state lifetime of $0.05\mu s$ is shorter than the average time between collisions, $0.16\mu s$. This calculated value of $74^{\circ}K$ for an average rotational temperature increase due to an excitation collision is in good agreement with the observation that spectroscopically measured temperatures at the start of the spark are $60^{\circ}K$ higher than the ambient gas temperature. If this interpretation is correct, then actual gas temperatures can be expected to be $60^{\circ}K$ lower than the spectroscopically measured temperature.

Until these points are fully explained, little can be said about the

interpretation of average spark temperatures (Figure 13) and relative spark diameters (Figure 16) for other combinations of spark energy and static pressure. It is clear, however, that nonequilibrium effects will be the most pronounced for cases of lowest pressure or shortest spark duration.

REFERENCES

1. Crompton, R. W. and Sutton, D.J., 1952, "Diffusion of Slow Electrons in Nitrogen and Hydrogen", Proceedings of The Royal Society of London, Series A Vol. 215, p. 467.

2. Cunningham, J. W. and Dicks, J. B., 1964, "A Microwave Method of Measuring Plasma Velocity", Proceedings of The Third Hypervelocity Techniques Symposium, Denver, March 1964.

3. Fuller, W. H. Jr., 1965, Private Communication.

4. Gerjuoy, E. and Stein, S., 1955, "Rotational Excitation by Slow Electrons", Physical Review, Vol. 97, p. 1671.

5. Haas, R., 1957, "Unterschunger iber den Energieverlust Langsamer Elektronen in Stickstoff", Z. Physick, Vol. 148, p. 177.

6. Hertzberg, G., 1950, Spectra of Diatomic Molecules, D. van Nostrand and Co., New York.

7. Karamcheti, K., Vali, W., Kyser, J. B., and Rasmussen, M. L.,1962, "Measurements of Pressure and Speed of Flow in a Spark-Heated Hypersonic Wind Tunnel", Arnold Engineering Development Center, AEDC-TDR-62-218.

8. Kyser, J. B., 1964, "Tracer-Spark Technique for Velocity Mapping of Hypersonic Flow Fields", AIAA Journal, Vol. 2, p. 393.

9. Massey, H. S. W. and Burhop, E. H. S., 1952, Electronic and Ionic Impact Phenomena, Oxford University Press.

10. Nicholls, R. W., 1964, "Transition Probabilities of Aeronomically Important Spectra", Annales de Geophysique, Tome 20, p. 144.

11. Rudinger, G., 1964, Comments on "Tracer-Spark Technique for Velocity Mapping of Hypersonic Flow Fields", AIAA Journal, Vol. 2, p. 1517.

12. Shultz, C. J., 1949, "Measurement of Excitation of N_2, CO, and He by Electron Impact", Physical Review, Vol. 116, p. 1141.

13. Townsend, J. S. and Bailey, V. A., 1921, "The Motion of Electrons in Gases", Philosophical Magazine, Vol. 42, p. 873.

14. von Engle, A., 1955, Ionized Gases, Oxford University Press.

TABLE I ELECTRON CHARACTERISTICS AS A FUNCTION OF ELECTRIC FIELD STRENGTH

ELECTRIC FIELD STRENGTH V/CM/MM HG	MEAN ENERGY ELECTRON VOLTS	MEAN VELOCITY CM/SEC X 10^{-7}	DRIFT VELOCITY CM/SEC X 10^{-5}	MEAN FREE PATH CM X 10^{2}	FRACTIONAL ENERGY TRANSFER X 10^{4}	SOURCE
0.1	0.181	2.51	2.9	4.54	3.11	Crompton and Sutton
0.2	0.298	3.23	3.7	3.72	3.07	" " "
0.3	0.406	3.75	4.2	3.28	2.90	" " "
0.4	0.507	4.20	4.8	3.15	3.03	" " "
0.5	0.604	4.58	5.3	3.05	3.10	" " "
0.6	0.682	4.88	5.8	2.95	3.28	" " "
0.7	0.753	5.12	6.3	2.89	3.52	" " "
0.8	0.823	5.35	6.9	2.89	3.86	" " "
0.9	0.872	5.52	7.4	2.84	4.20	" " "
1.0	0.920	5.67	7.9	2.80	4.52	" " "
1.2	1.002	5.92	8.9	2.74	5.27	" " "
1.5	1.092	6.17	10.5	2.68	6.73	" " "
1.8	1.174	6.40	12.0	2.66	8.20	" " "
2.0	1.226	6.55	12.9	2.63	9.05	" " "
3.0	1.390	6.96	17.4	2.52	14.5	" " "
4.0	1.509	7.25	21.6	2.44	20.6	" " "
5.0	1.602	7.48	25.4	2.37	26.9	" " "
10.0	1.874	8.08	43.4	2.19	66.9	" " "
15.0	2.042	8.43	59.0	2.07	114.	" " "
20.0	2.221	8.70	74.4	2.04	166.	" " "
20.0	2.25	8.85	86.	1.86	-	Townsend and Bailey
30.0	2.77	9.8	117.	1.85	-	" " "
40.0	3.37	10.83	146.	1.82	-	" " "
50.0	4.08	11.94	171.	1.80	-	" " "
60.0	4.78	12.9	193.	1.78	-	" " "
100.0	6.82	15.4	250.	1.75	-	" " "

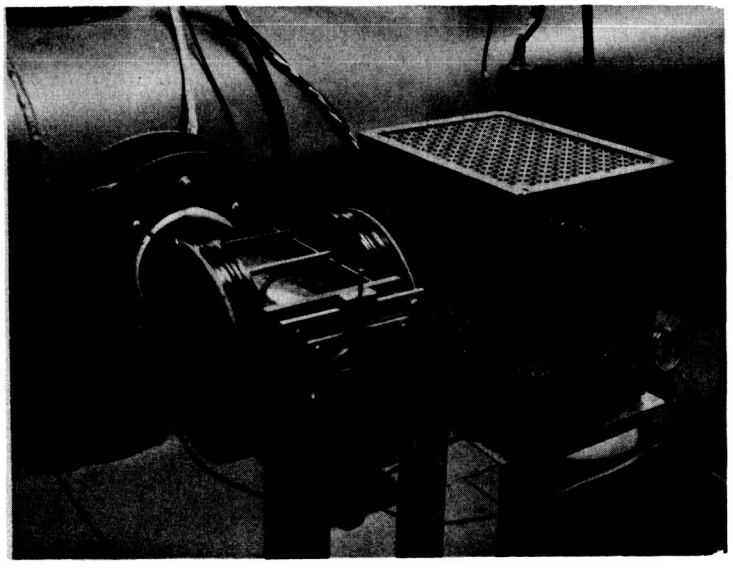

a) Static-Test Chamber and Spark Circuit

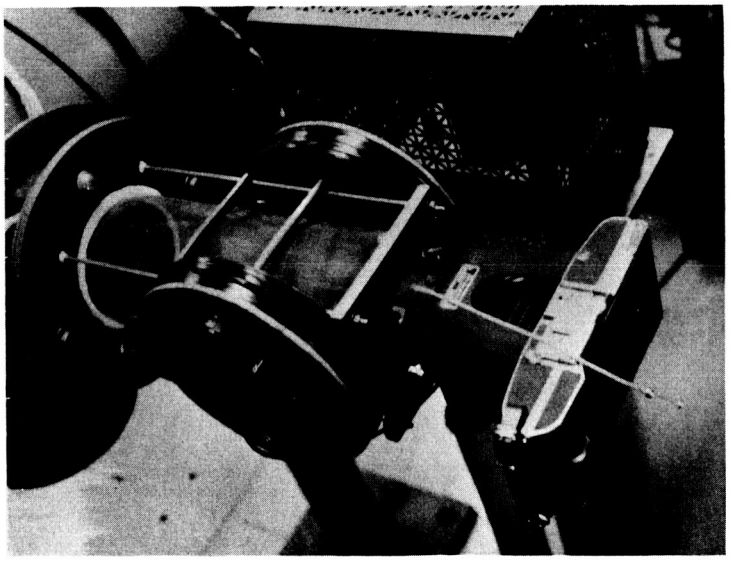

b) Camera Mounted on Static-Test Chamber

FIG. 1 PHOTOGRAPHS OF STATIC-TEST CHAMBER

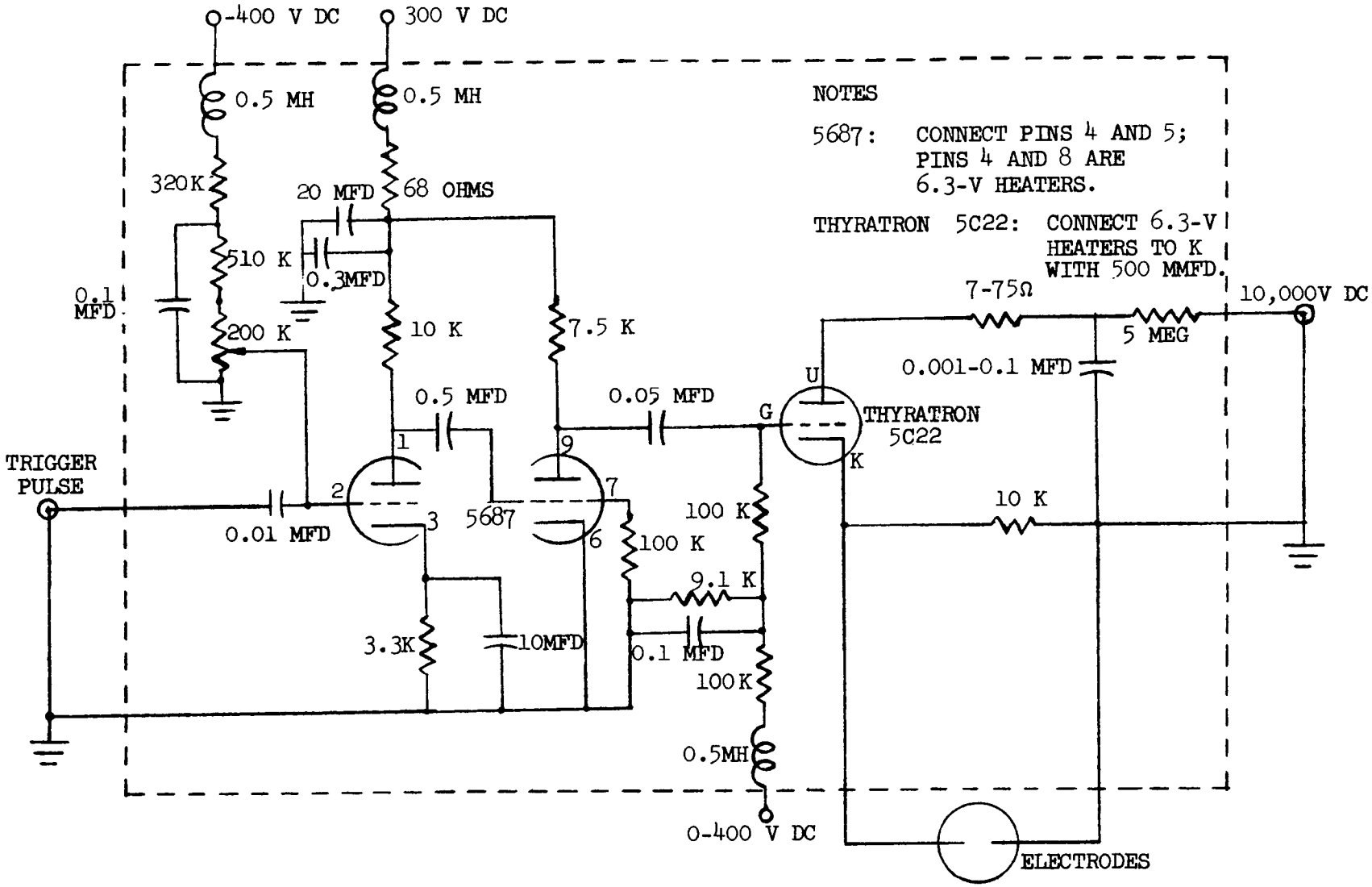

FIG. 2 DIAGRAM OF CIRCUIT USED TO PRODUCE SPARKS

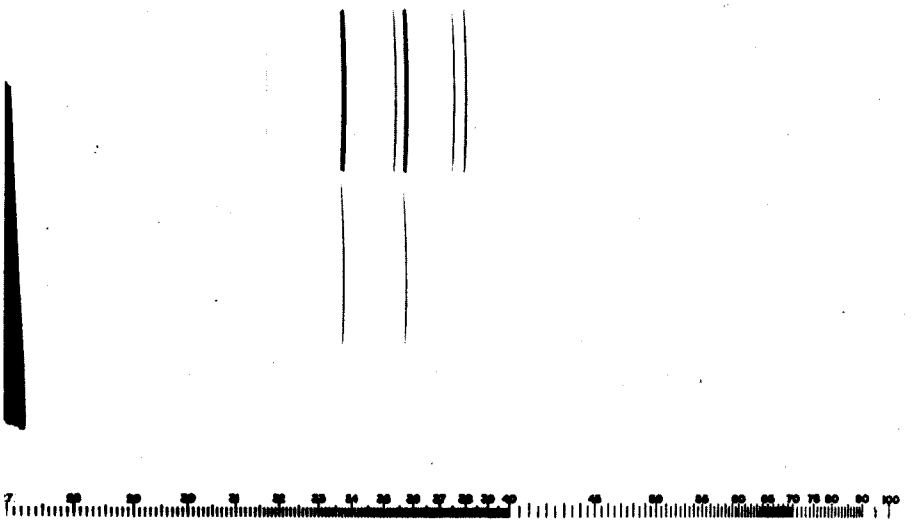

a) 0-Gauss Magnetic Field

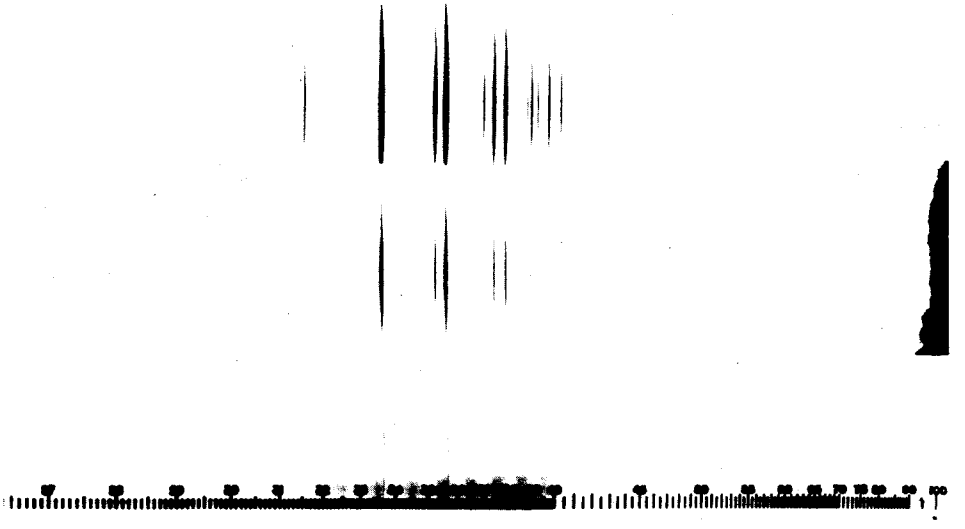

b) 655-Gauss Magnetic Field

FIG. 3 SPECTRA OF SPARK IN NITROGEN
0.5-JOULE SPARK, 1 MM HG

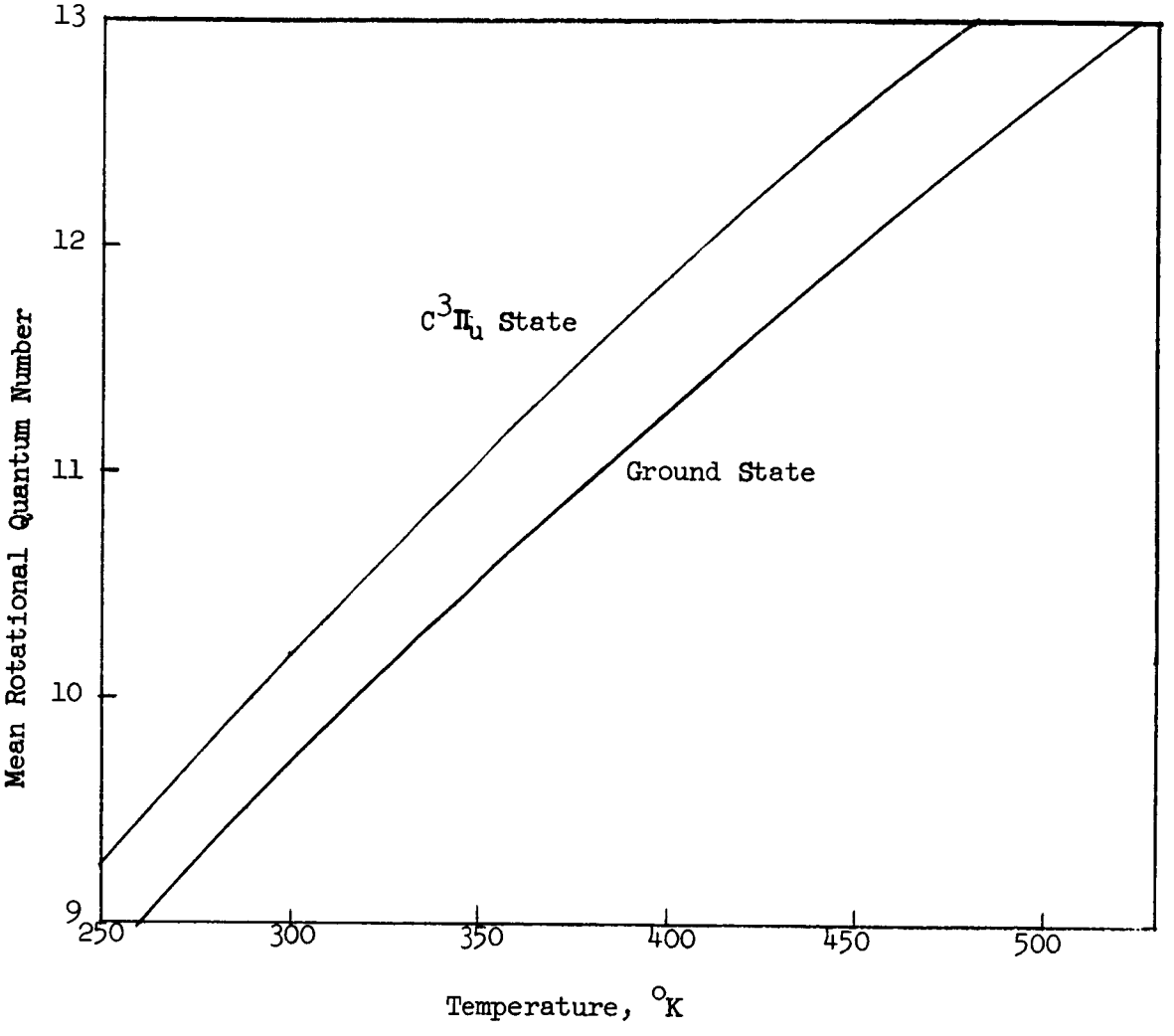

FIG. 4 ROTATIONAL QUANTUM NUMBER REPRESENTED BY AVERAGE MOLECULAR ROTATIONAL KINETIC ENERGY

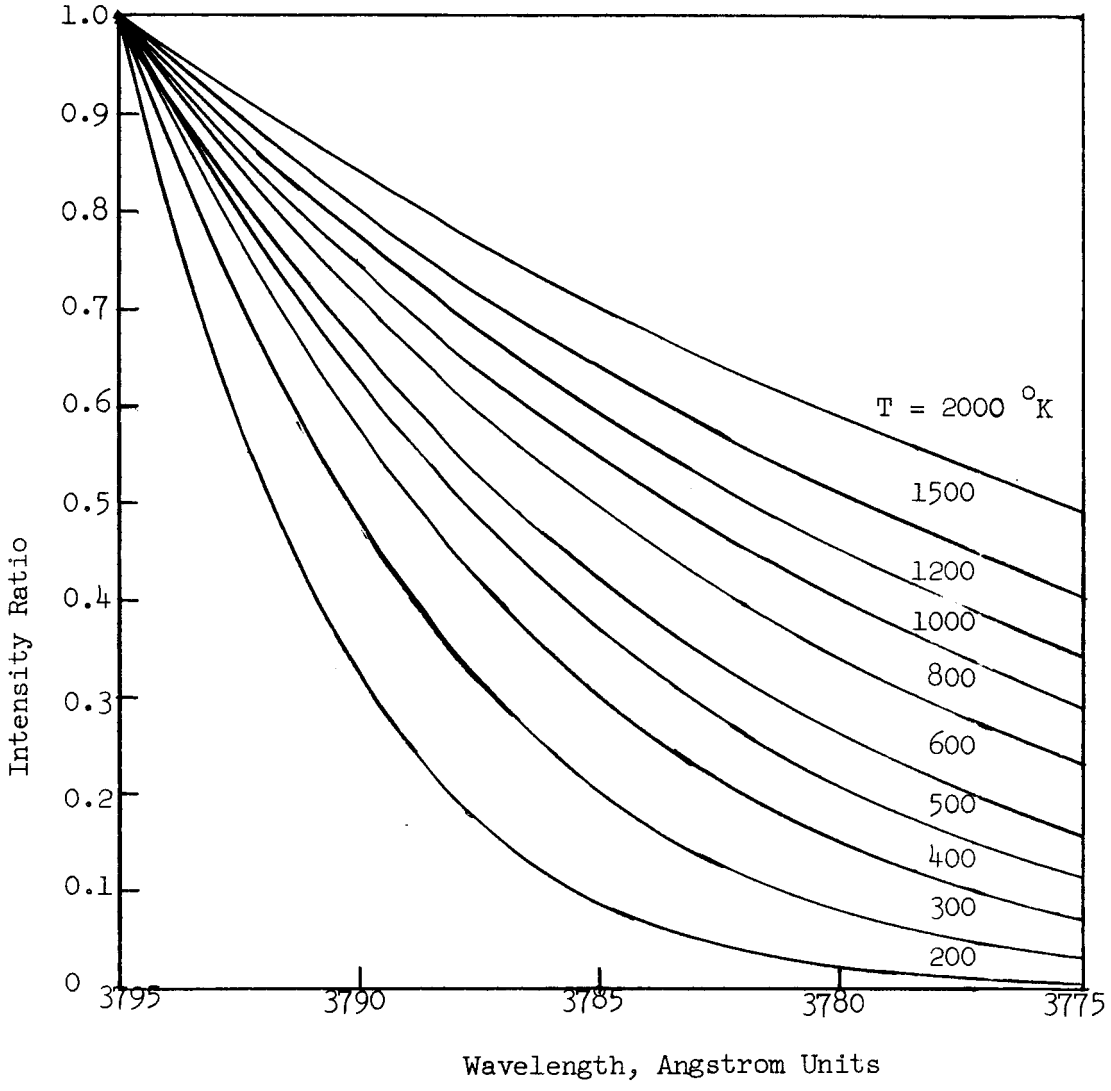

FIG. 5 EFFECT OF ROTATIONAL TEMPERATURE ON BAND-INTENSITY DISTRIBUTION

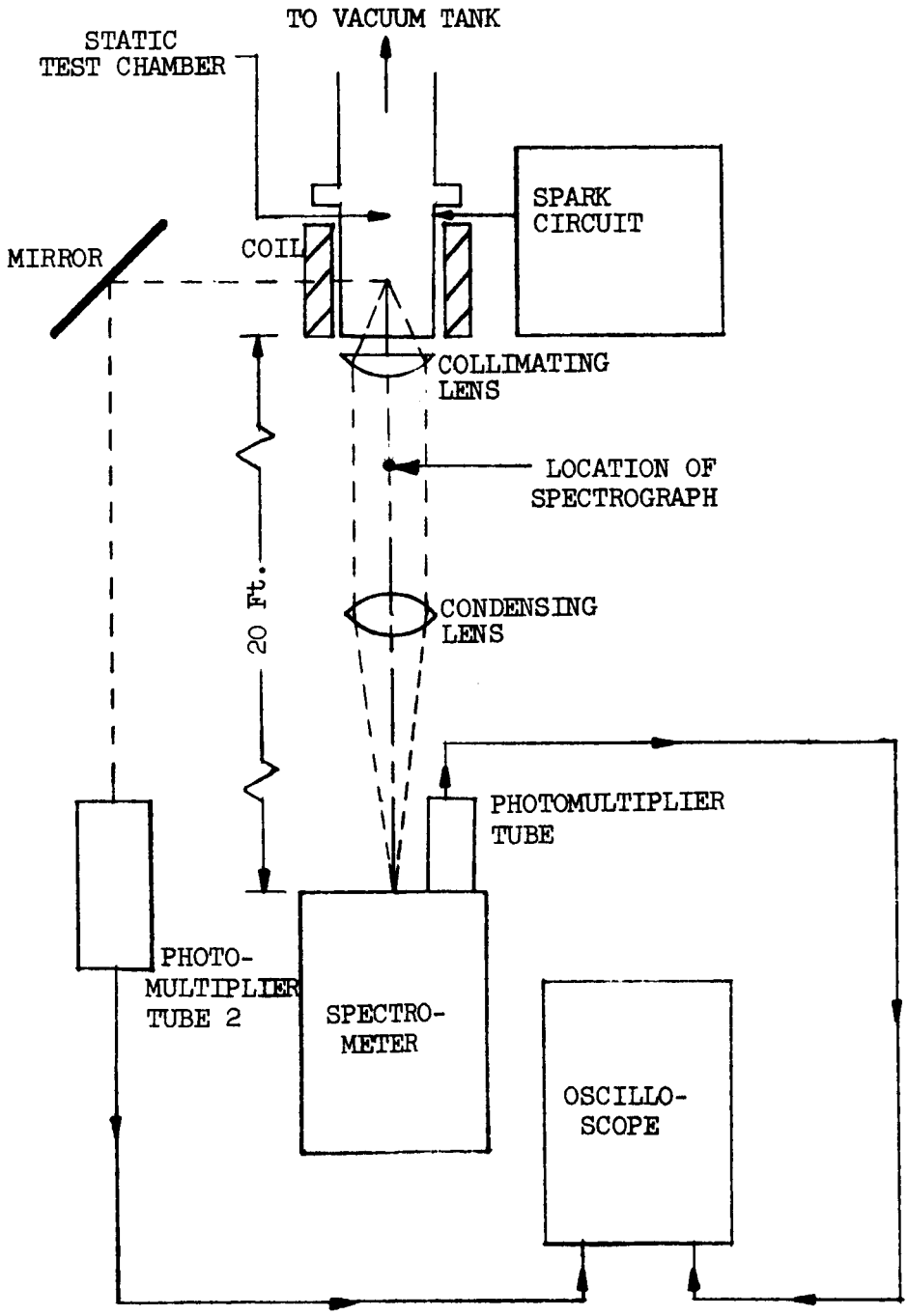

FIG. 6 APPARATUS FOR MAKING SPARK-TEMPERATURE MEASUREMENTS

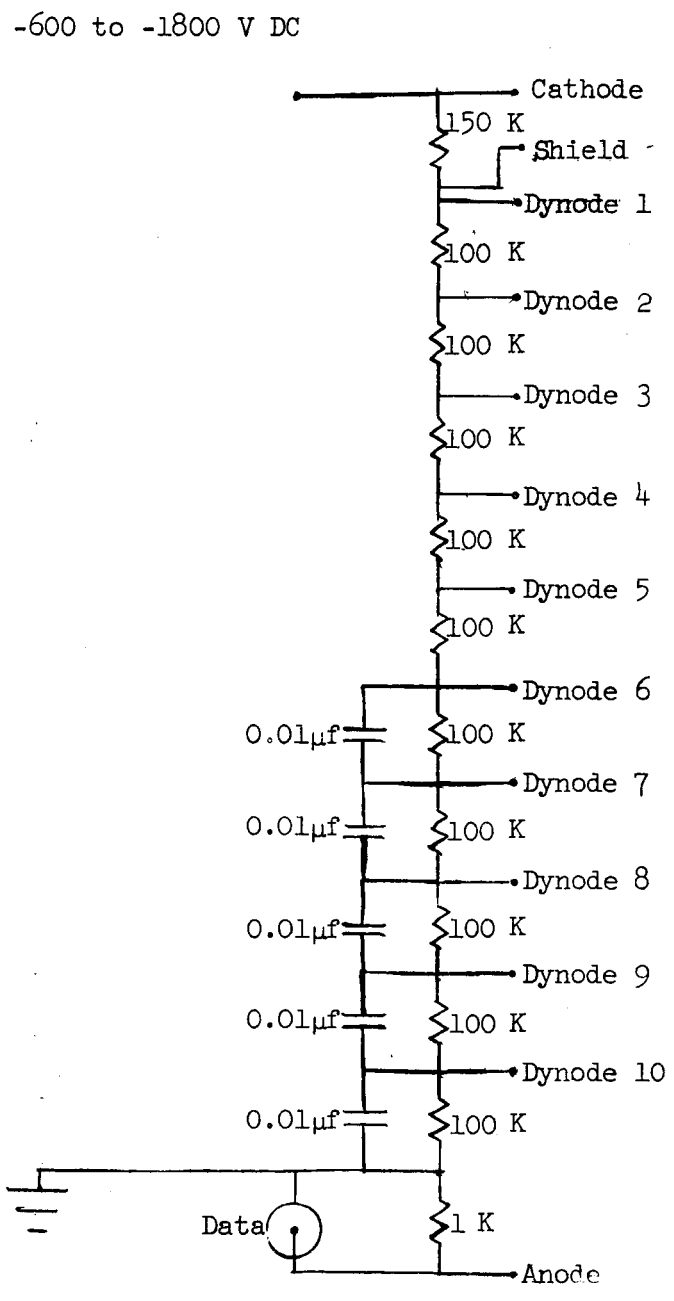

FIG. 7 PHOTOMULTIPLIER CIRCUIT

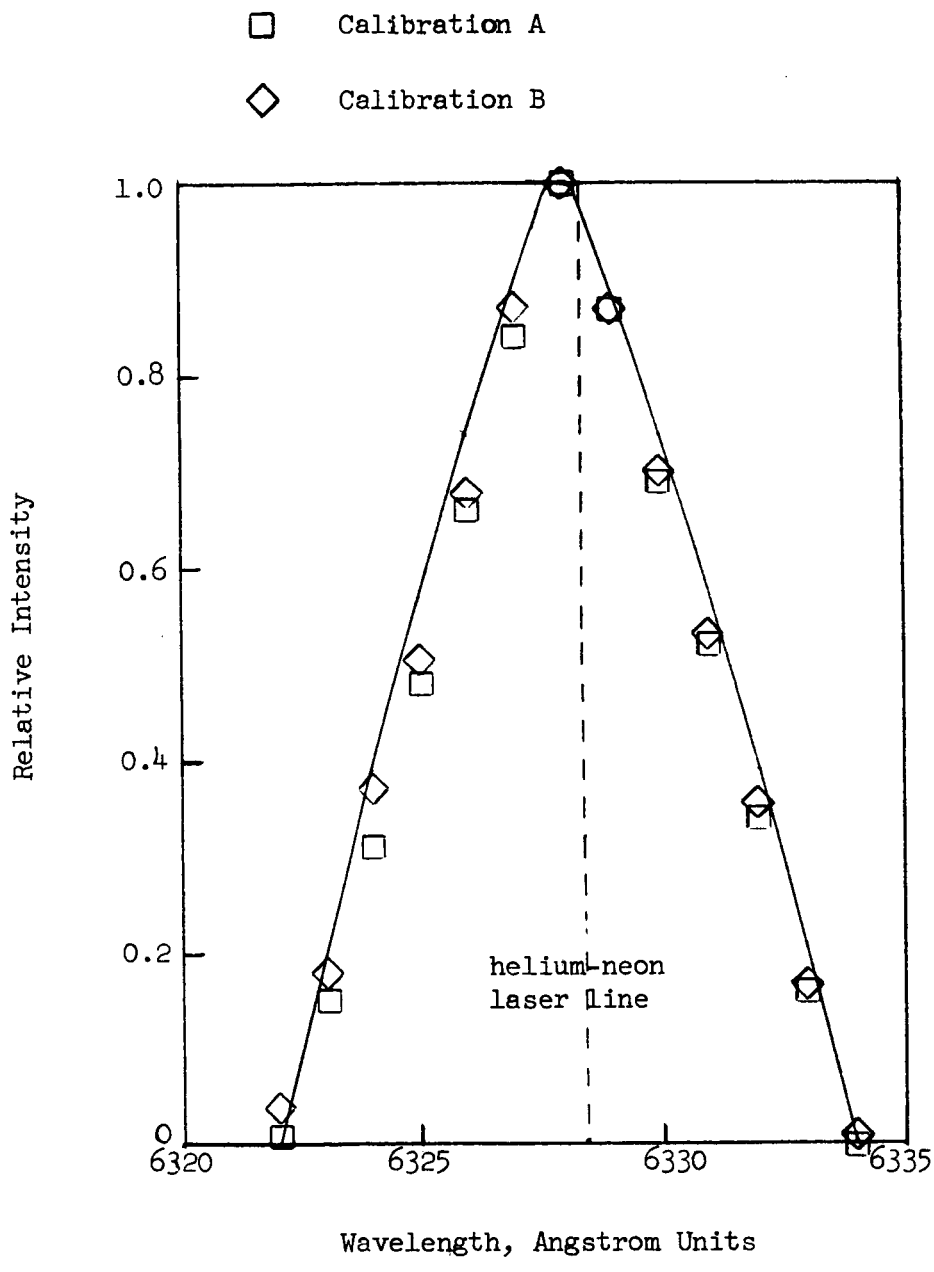

FIG. 8 INSTRUMENT PROFILE CALIBRATION
400μ SLIT WIDTH

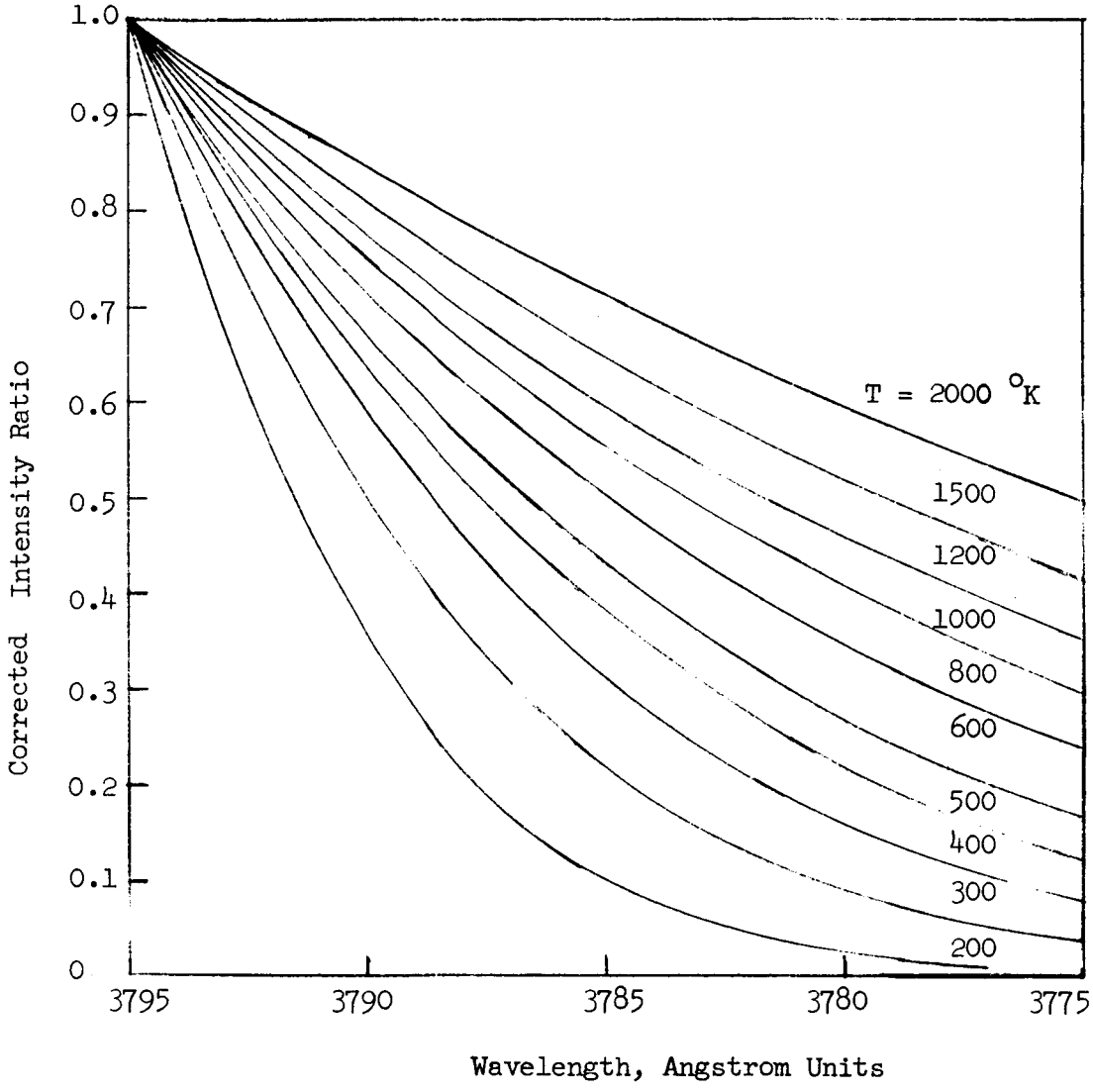

FIG. 9 CORRECTED BAND-INTENSITY DISTRIBUTION
400μ SLIT WIDTH

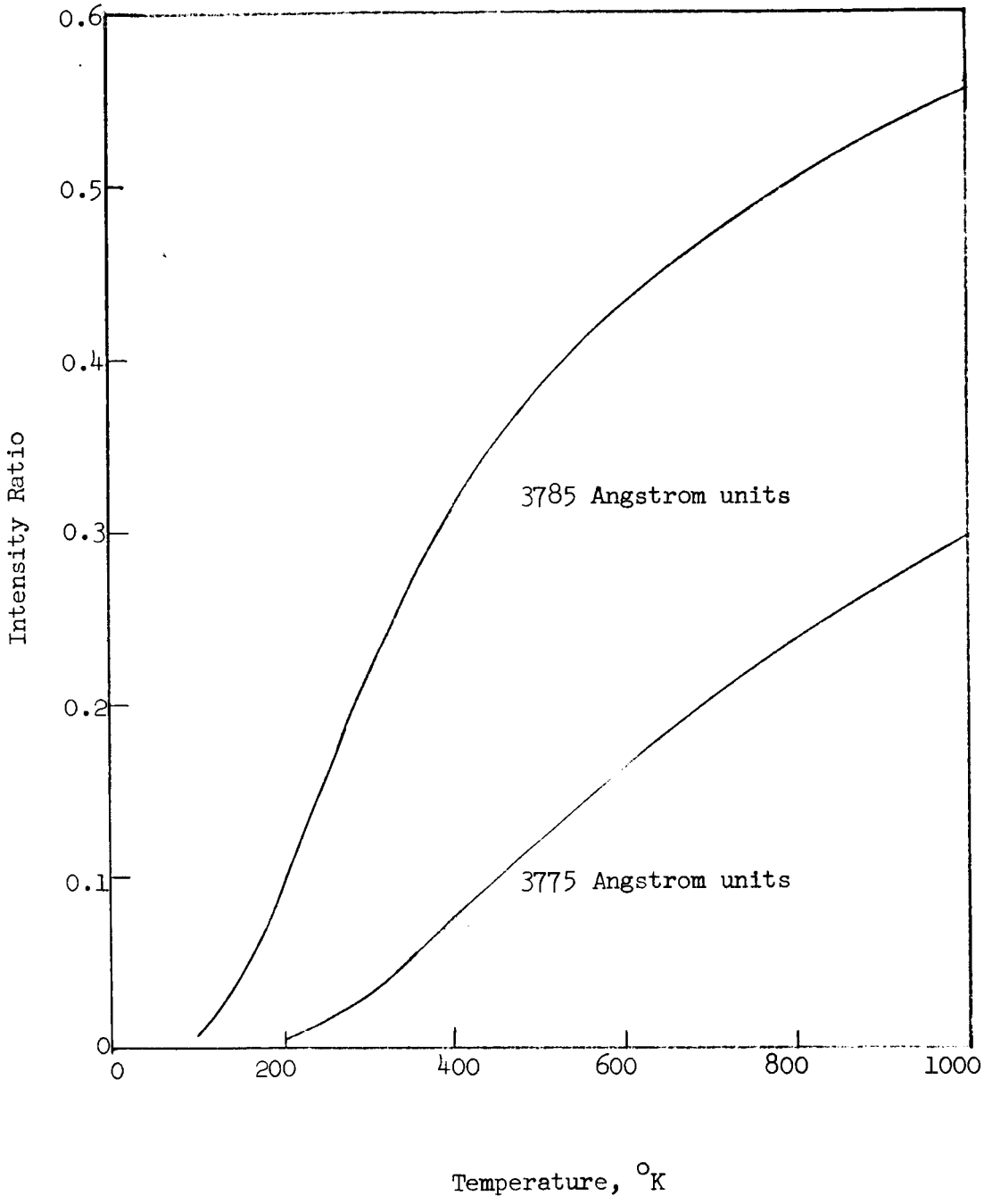

FIG. 10 INTENSITY RATIO VS. TEMPERATURE:
400μ SLIT WIDTH

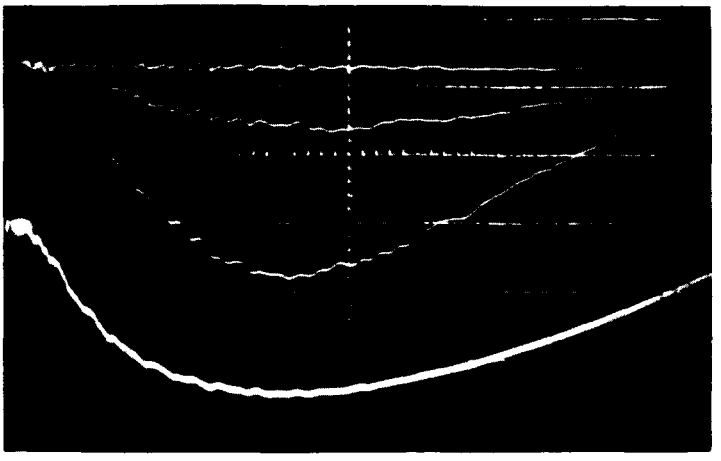

Upper Trace: Spectrometer Output, 0.02 V/cm
Lower Trace: Monitor
Time Base: 0.2μs/cm

a) 5.0-Joule Spark

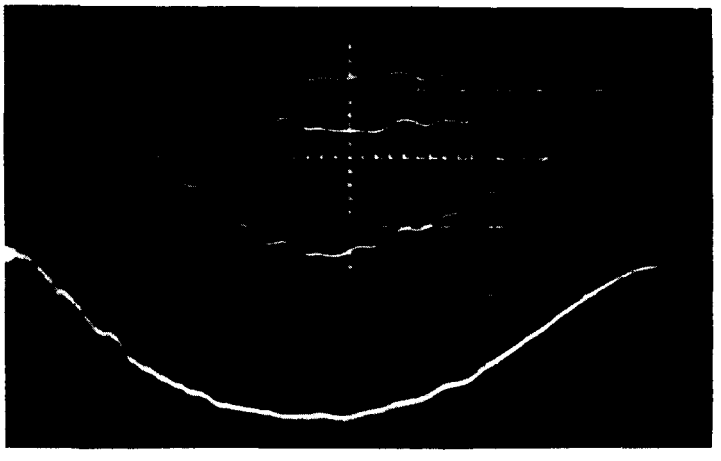

Upper Trace: Spectrometer Output, 0.02 V/cm
Lower Trace: Monitor
Time Base: 0.1μs/cm

b) 0.5-Joule Spark

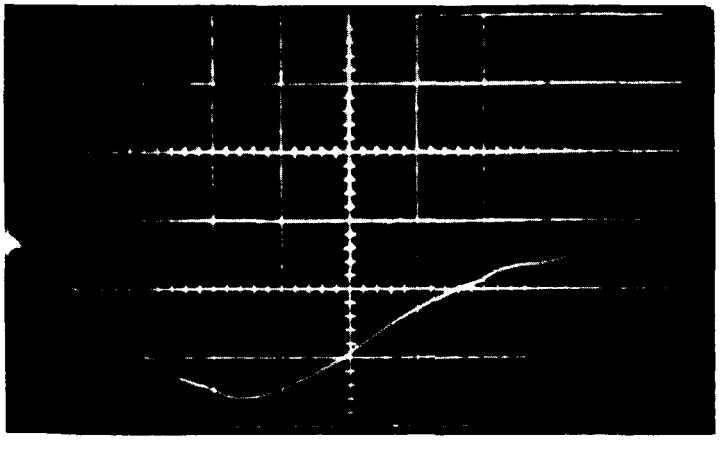

Upper Trace: Spectrometer Output, 0.02 V/cm
Lower Trace: Monitor
Time Base: 0.04μs/cm

c) 0.05-Joule Spark

FIG. 11 OSCILLOSCOPE TRACES OF SPECTROMETER OUTPUT
1 MM HG, 0-GAUSS MAGNETIC FIELD

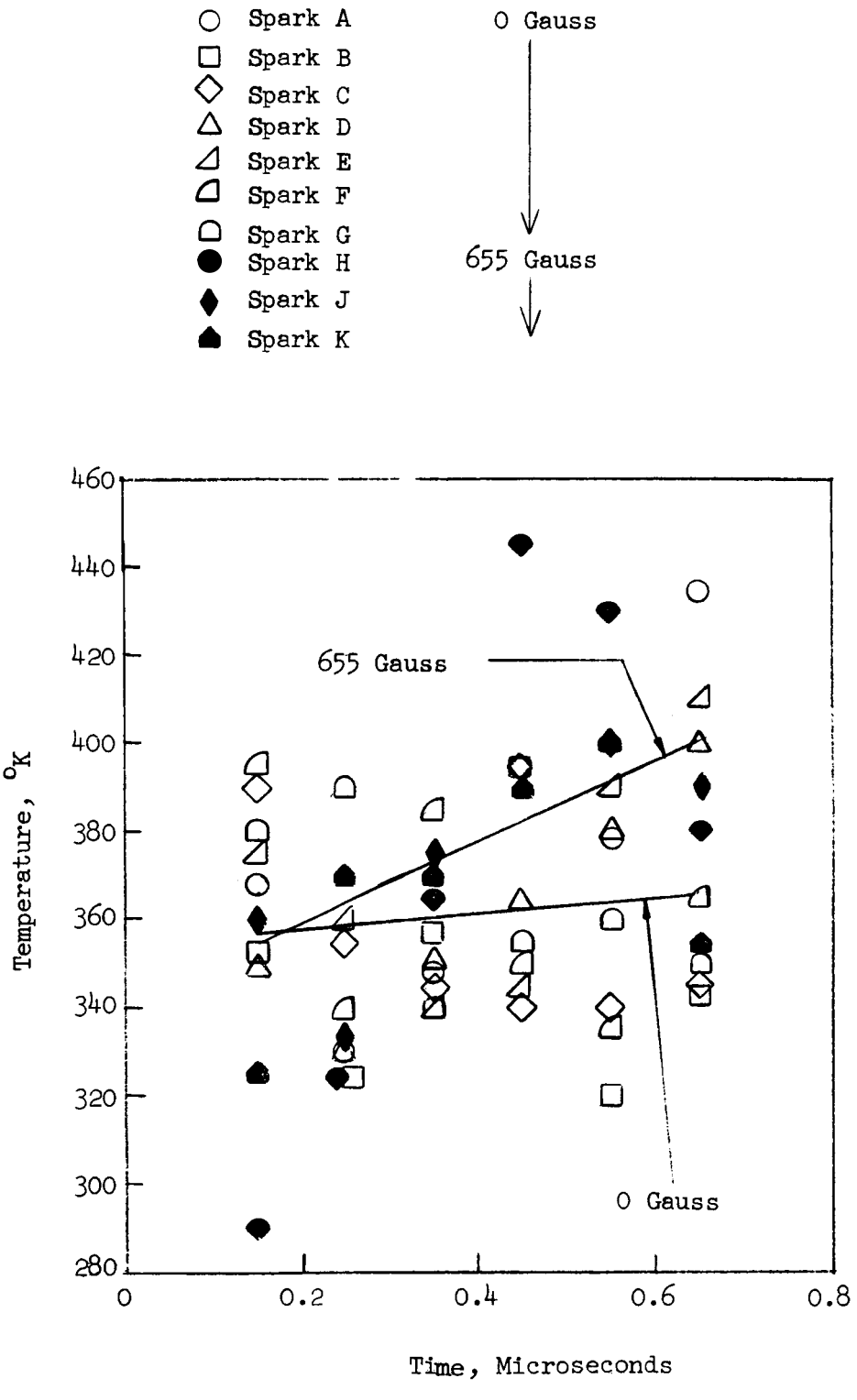

FIG. 12 TIME-RESOLVED SPARK-TEMPERATURE MEASUREMENTS
0.5 JOULE SPARK, 1 MM HG

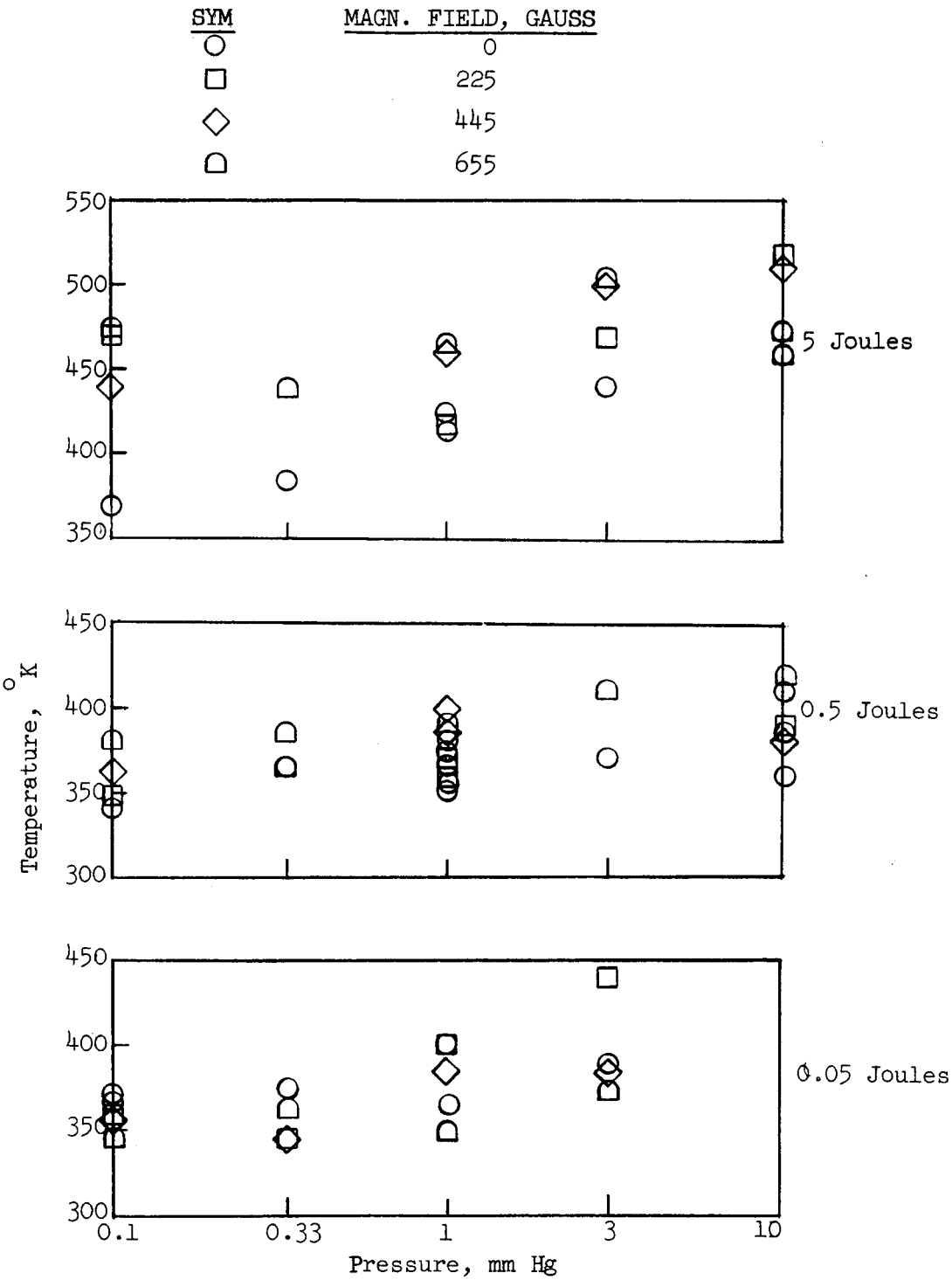

FIG. 13 AVERAGE SPARK TEMPERATURE

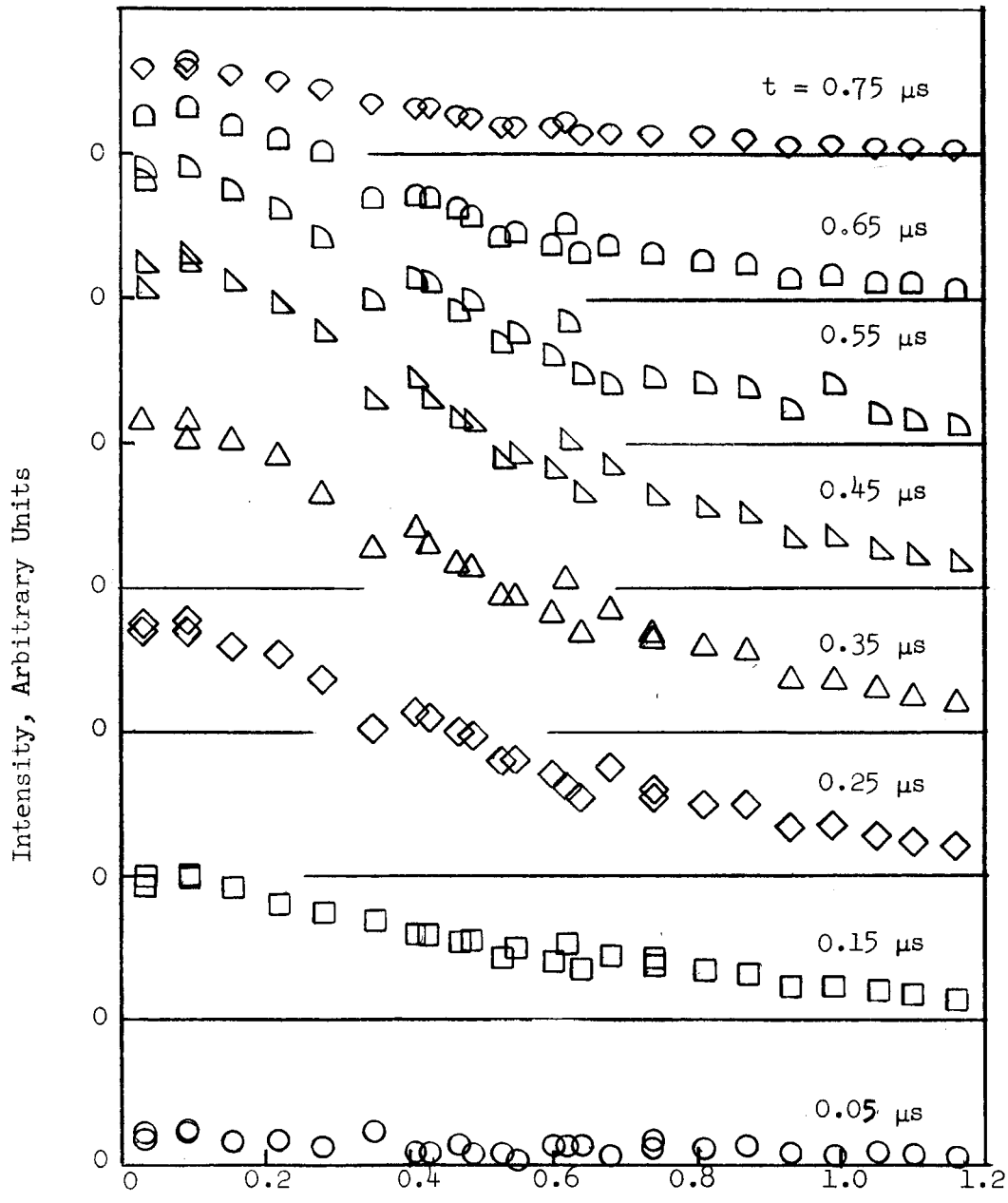

(a) 0.5 Joule, 1 mm, 0 Gauss

FIG. 14 TIME-RESOLVED SPARK INTENSITY PROFILES

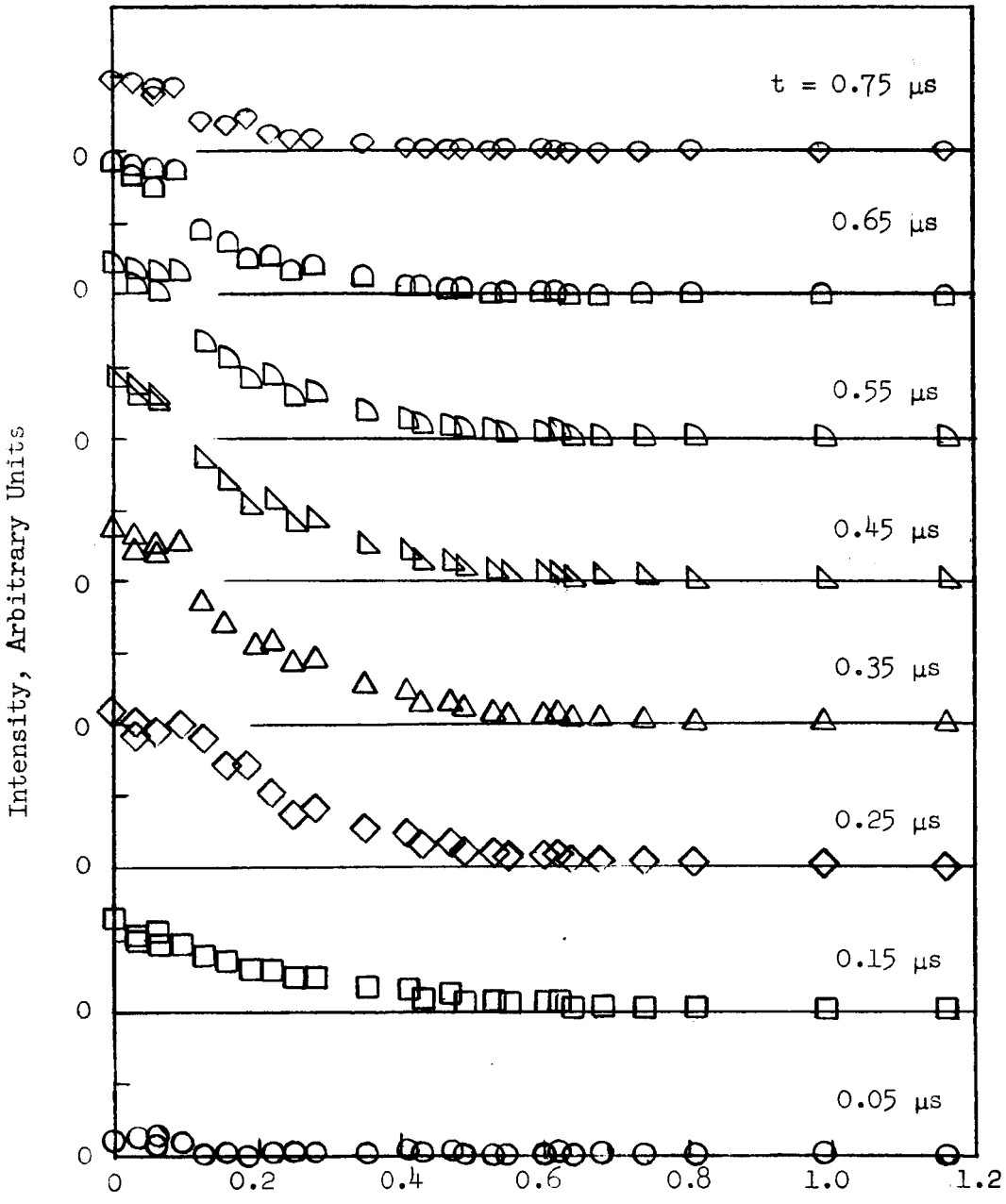

(b) 0.5 Joule, 1 mm, 655 Gauss

FIG. 14 CONCLUDED

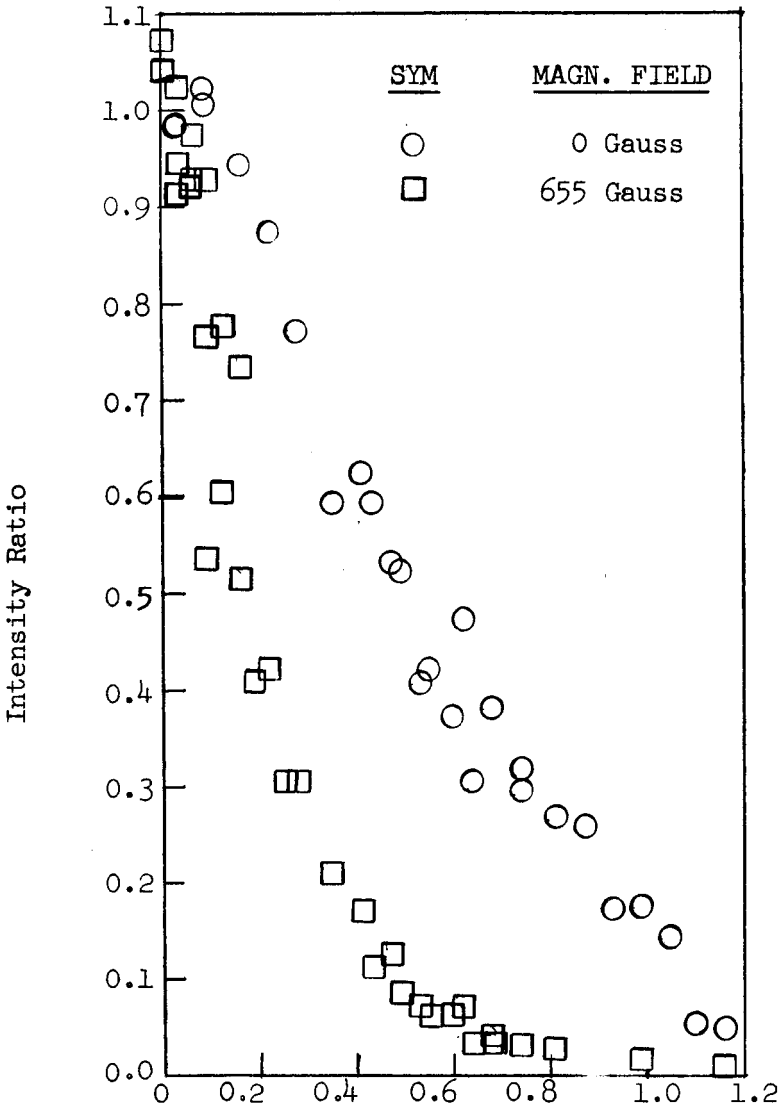

FIG. 15 INTEGRATED SPARK-INTENSITY PROFILES

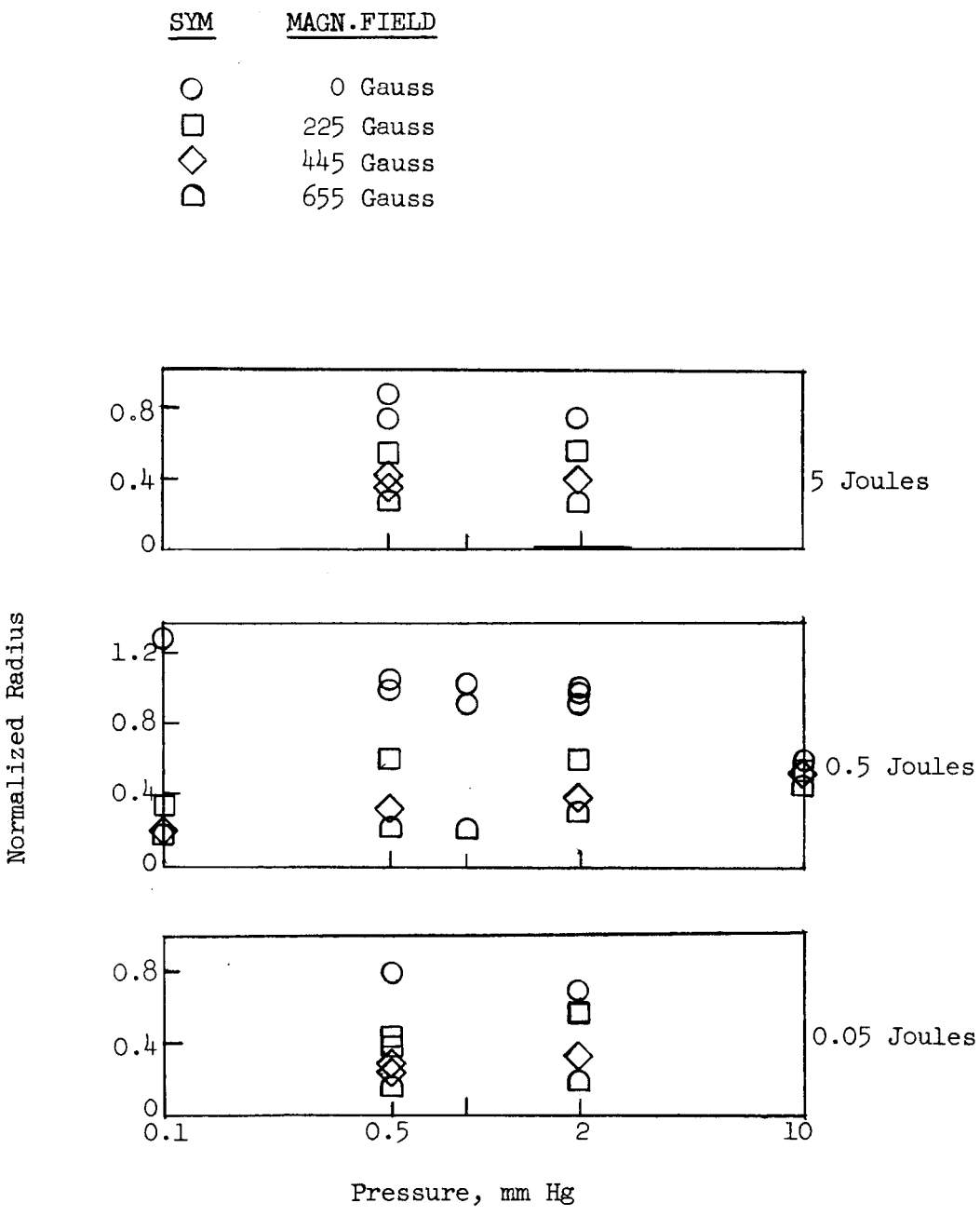

FIG. 16 NORMALIZED SPARK RADIUS

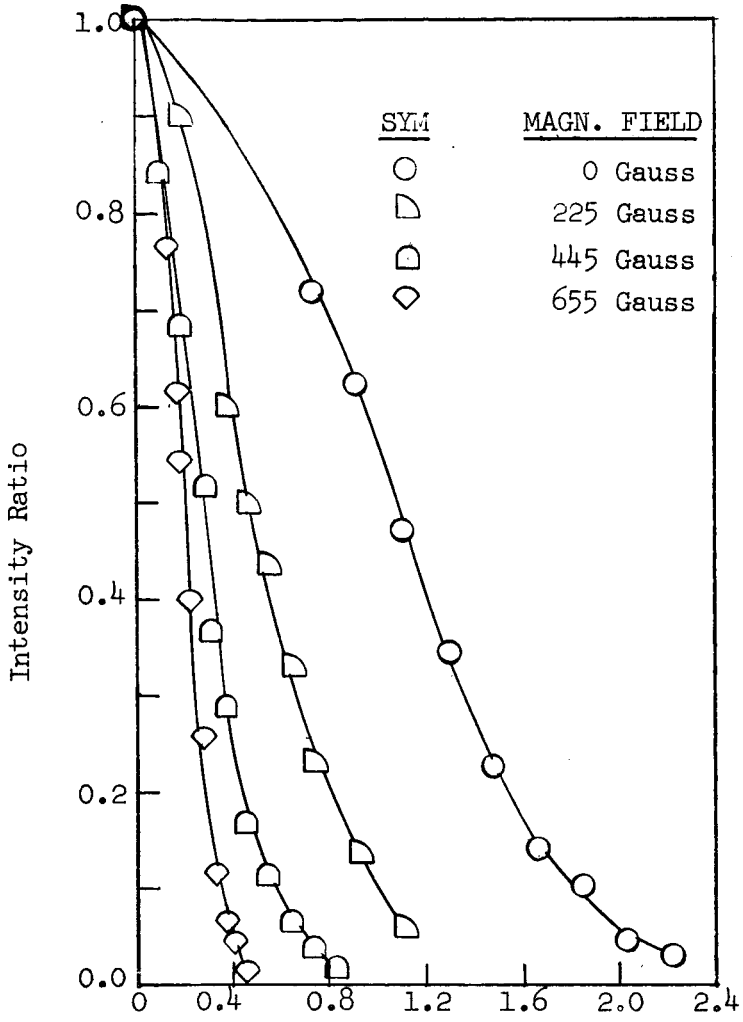

FIG. 17 SPARK INTENSITY PROFILES OBTAINED FROM PHOTOGRAPHIC DATA

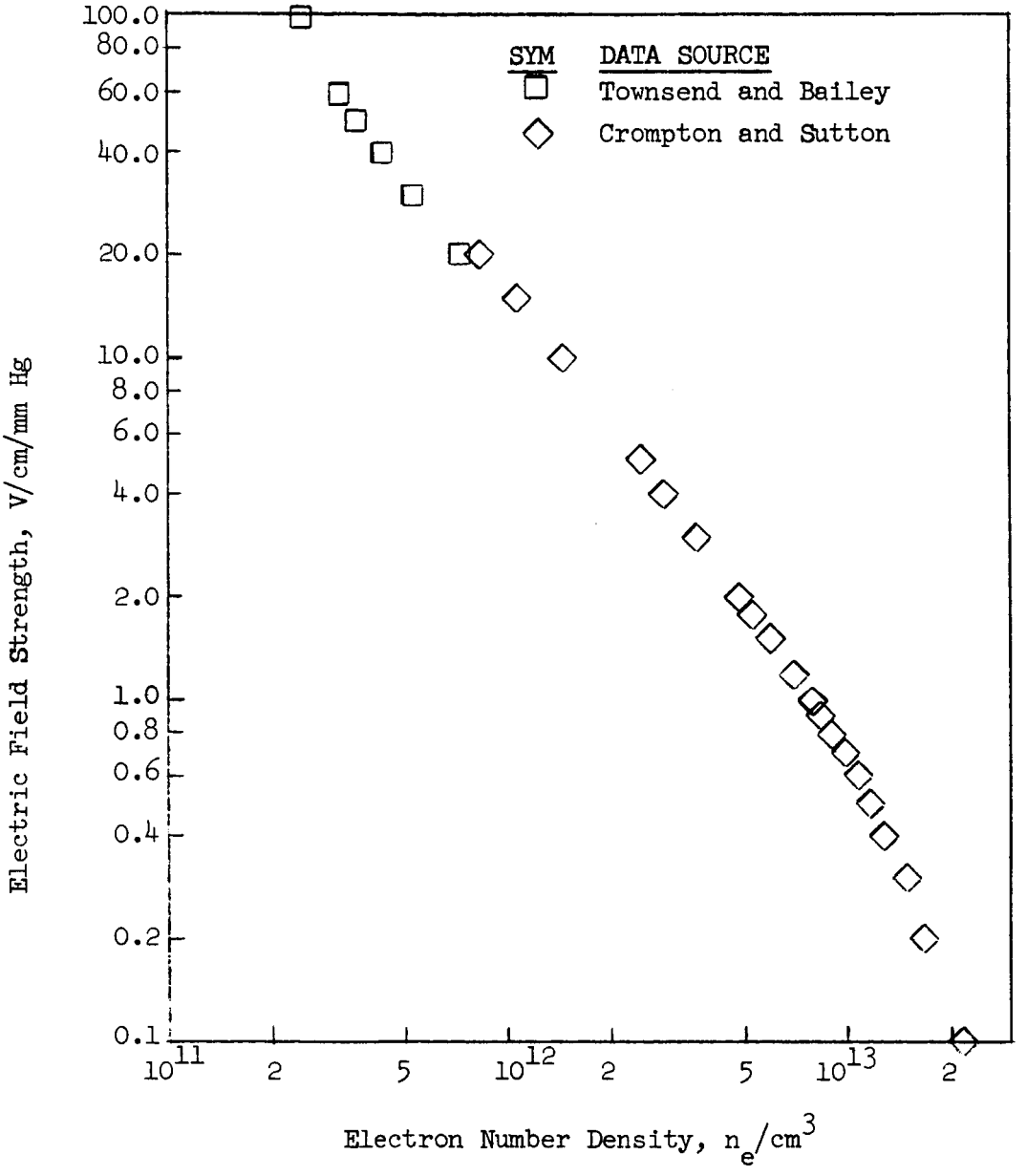

FIG. 18 ELECTRON NUMBER DENSITY REQUIRED TO CONDUCT A CURRENT DENSITY OF 1.0 AMP/CM^2

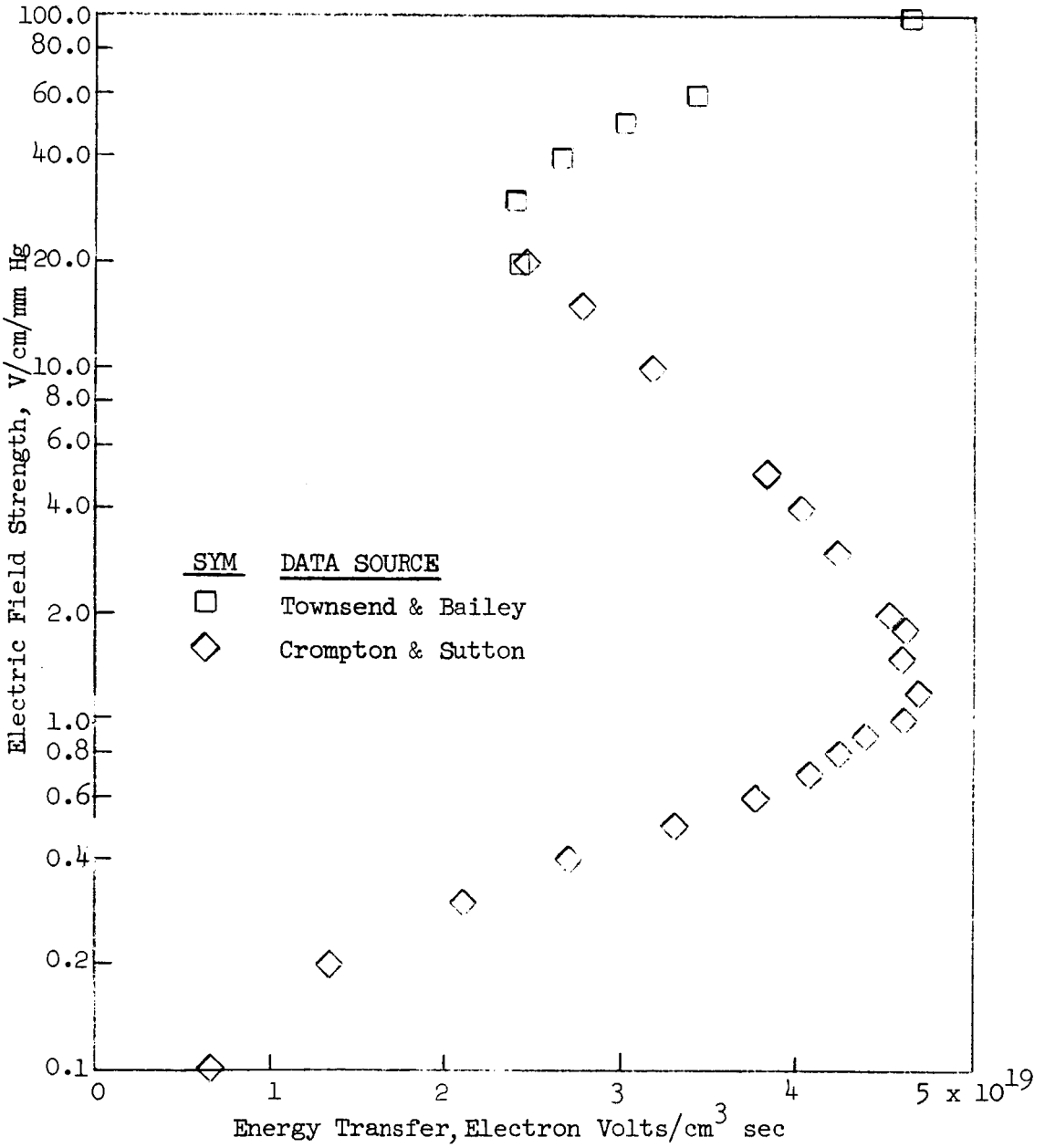

FIG. 19 ENERGY TRANSFER TO ACTIVE DEGREES OF FREEDOM FOR A CURRENT DENSITY OF 1.0 AMP/CM^3